4-6-2021

Metabolic modulation by CDK4/6 inhibitor promotes chemokine-mediated recruitment of T cells into mammary tumors

Roman V Uzhachenko

Vijaya Bharti

Zhufeng Ouyang

Ashlyn Blevins

Stacey Mont

See next page for additional authors

Authors

Roman V Uzhachenko, Vijaya Bharti, Zhufeng Ouyang, Ashlyn Blevins, Stacey Mont, Nabil Saleh, Hunter A Lawrence, Chengli Shen, Sheau-Chiann Chen, Gregory D Ayers, David G DeNardo, Carlos Arteaga, Ann Richmond, and Anna E Vilgelm

Cell Reports

Article

Metabolic modulation by CDK4/6 inhibitor promotes chemokine-mediated recruitment of T cells into mammary tumors

Graphical abstract

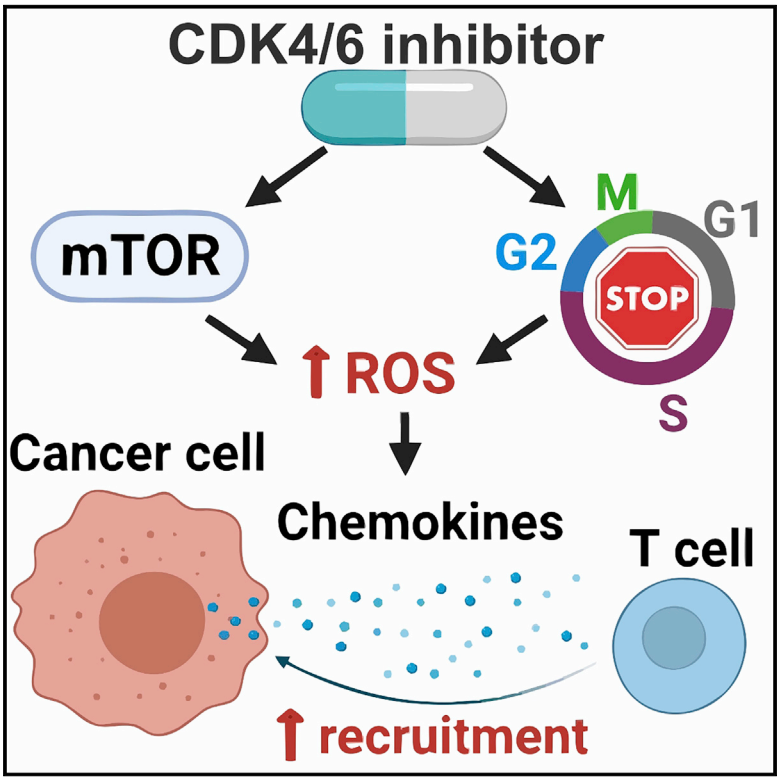

Authors

Roman V. Uzhachenko, Vijaya Bharti, Zhufeng Ouyang, ..., Carlos Arteaga, Ann Richmond, Anna E. Vilgelm

Correspondence

anna.vilgelm@osumc.edu

In brief

Inhibitors of cell cycle kinases CDK4/6 delay progression of metastatic breast cancer; however, they do not eliminate tumors. Uzhachenko et al. report that metabolic changes in CDK4/6 inhibitor-treated cancer cells make them vulnerable to T cell therapies. These data highlight potential utility of CDK4/6 inhibitors to overcome immunotherapy resistance.

Highlights

- Breast cancer cells treated with CDK4/6 inhibitor secrete chemokines CCL5 and CXCL10
- Chemokine induction is associated with deregulated mTOR, metabolic stress, and ROS
- Chemokines induced by CDK4/6 inhibitor facilitate T cell infiltration into tumors
- Chemokines induced by CDK4/6 inhibitor augment adoptive T cell therapy

Uzhachenko et al., 2021, Cell Reports *35*, 108944
April 6, 2021
https://doi.org/10.1016/j.celrep.2021.108944

CellPress

Cell Reports

CellPress
OPEN ACCESS

Article

Metabolic modulation by CDK4/6 inhibitor promotes chemokine-mediated recruitment of T cells into mammary tumors

Roman V. Uzhachenko,[1,2] Vijaya Bharti,[1,2] Zhufeng Ouyang,[1,2] Ashlyn Blevins,[3] Stacey Mont,[3] Nabil Saleh,[3] Hunter A. Lawrence,[3] Chengli Shen,[1] Sheau-Chiann Chen,[4] Gregory D. Ayers,[4] David G. DeNardo,[5] Carlos Arteaga,[6,7] Ann Richmond,[3,8] and Anna E. Vilgelm[1,2,9,*]

[1]Comprehensive Cancer Center - James, The Ohio State University Wexner Medical Center, Columbus, OH 43210, USA
[2]Department of Pathology, The Ohio State University Wexner Medical Center, Columbus, OH 43210, USA
[3]Department of Pharmacology, Vanderbilt University School of Medicine, Nashville, TN 37212, USA
[4]Department of Biostatistics, Vanderbilt University Medical Center, Nashville, TN 37212, USA
[5]Department of Medicine, Washington University St. Louis, School of Medicine, St. Louis, MO 63110, USA
[6]Simmons Comprehensive Cancer Center, University of Texas Southwestern Medical Center, Dallas, TX 75390, USA
[7]Department of Internal Medicine, University of Texas Southwestern Medical Center, Dallas, TX 75390, USA
[8]Department of Veterans Affairs, Tennessee Valley Healthcare System, Nashville, TN 37212, USA
[9]Lead contact
*Correspondence: anna.vilgelm@osumc.edu
https://doi.org/10.1016/j.celrep.2021.108944

SUMMARY

Inhibitors of cyclin-dependent kinases 4 and 6 (CDK4/6i) delay progression of metastatic breast cancer. However, complete responses are uncommon and tumors eventually relapse. Here, we show that CDK4/6i can enhance efficacy of T cell-based therapies, such as adoptive T cell transfer or T cell-activating antibodies anti-OX40/anti-4-1BB, in murine breast cancer models. This effect is driven by the induction of chemokines CCL5, CXCL9, and CXCL10 in CDK4/6i-treated tumor cells facilitating recruitment of activated $CD8^+$ T cells, but not Tregs, into the tumor. Mechanistically, chemokine induction is associated with metabolic stress that CDK4/6i treatment induces in breast cancer cells. Despite the cell cycle arrest, CDK4/6i-treated cells retain high metabolic activity driven by deregulated PI3K/mTOR pathway. This causes cell hypertrophy and increases mitochondrial content/activity associated with oxidative stress and inflammatory stress response. Our findings uncover a link between tumor metabolic vulnerabilities and anti-tumor immunity and support further development of CDK4/6i and immunotherapy combinations.

INTRODUCTION

CDK4 and CDK6 are cell cycle kinases that work in complex with cyclin D1 to phosphorylate tumor suppressor RB. Phosphorylation inhibits RB activity leading to its dissociation from E2F transcription factors. Free E2Fs, in turn, transactivate genes involved in DNA replication and cell cycle progression. Inhibitors of CDK4/6 (CDK4/6i), such as palbociclib, ribociclib, and abemaciclib, control tumor growth by blocking G1-to-S cell cycle transition in cancer cells. CDK4/6i are used for treatment of recurrent ER-positive, HER2-negative metastatic breast cancer (Cristofanilli et al., 2016; Turner et al., 2018).

Interestingly, several studies indicated that, in addition to direct effect on tumor cells, CDK4/6 inhibitors may influence immune cells in the tumor microenvironment (Petroni et al., 2020; Teh and Aplin, 2019). This includes suppression of regulatory T cell proliferation (Goel et al., 2017; Goel et al., 2016) and enhanced activation of tumor-infiltrating T cells (Deng et al., 2018; Schaer et al., 2018). Furthermore, CDK4/6i treatment may affect tumor cells in a way that may facilitate their recognition by the immune system (Goel et al., 2017). Accordingly, CDK4/6i was shown to augment immune checkpoint blockade therapy targeting PD-1/PD-L1 in mouse models (Deng et al., 2018; Goel et al., 2017; Schaer et al., 2018; Zhang et al., 2018).

These data suggest that CDK4/6i can promote activation of tumor-infiltrating T cells (TILs). However, breast cancer tumors often have low levels of TILs, which is referred to as "immunologically cold" tumor microenvironment. "Cold" tumors have tendency to respond poorly to anti-PD-1 therapy (Cristescu et al., 2018; Tumeh et al., 2014). Further, breast cancer patients with low TILs often have worse survival and have limited response to chemotherapy compared to patients with tumors that are highly infiltrated with T cells (Dushyanthen et al., 2015). Therefore, there is an unmet clinical need for therapeutic approaches that can improve recruitment of T cells into the tumor.

Trafficking, localization, and positioning of T cells is regulated by small proteins called chemokines (Chow and Luster, 2014). Chemokines secreted by tumor cells and by non-malignant cells within the tumor microenvironment (TME) play important role in shaping tumor immune landscape (Vilgelm and Richmond,

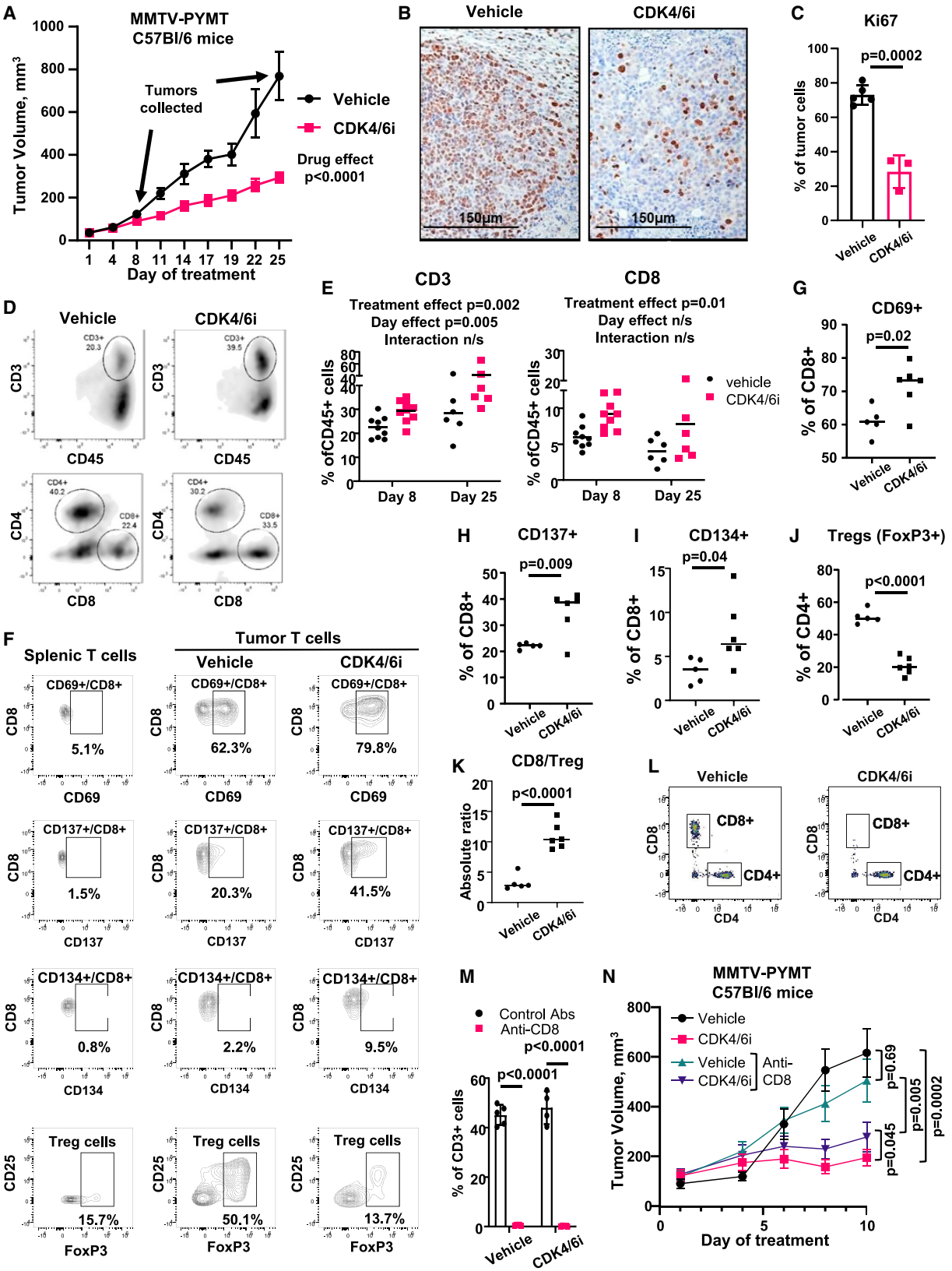

(legend on next page)

2019; Wellenstein and de Visser, 2018). A meta-analysis of 5,953 cancer specimens demonstrated positive correlation of CXCL9, CXCL10, and CXCL11 expression with density of tumor-infiltrating T and NK cells (Stoll et al., 2018). Similarly, CCR5 ligands, CCL4 and CCL5, were shown to facilitate recruitment of several anti-tumor immune cell types into the tumor including T cells and BATF3-dependent dendritic cells (Böttcher et al., 2018; Spranger et al., 2017; Vilgelm et al., 2015a). And vice versa, low expression of CCR5 ligands (CCL3, CCL4, CCL5) and CXCR3 ligands (CXCL9 and CXCL10) has been linked with limited T cells infiltration (Harlin et al., 2009). Importantly, chemokine expression is associated with effectiveness of immune checkpoint therapy (e.g., anti-PD1 and anti-PD-L1), as reviewed by Ayers et al. (2017) and Nagarsheth et al. (2017). Here, we investigated the role of chemokines in CDK4/6i-mediated modulation of tumor immune microenvironment.

RESULTS

CDK4/6 inhibitor increases levels of T cells in mammary tumors

We used a MMTV-PYMT murine mammary carcinoma model to study the effect of CDK4/6i palbociclib on tumor immune microenvironment. Transgenic MMTV-PYMT mice develop aggressive metastatic mammary tumors between 8 and 12 weeks of age (Guy et al., 1992) that recapitulate luminal BC subtype and express ERα and progesterone receptor (PR) similarly to human hormone receptor-positive luminal BC (Lin et al., 2003). Similar to human BC, PYMT tumors are not highly immunogenic based on virtually identical survival curves of PYMT mice on wild-type and T cell-deficient ($Rag^{-/-}$) backgrounds (DeNardo et al., 2009). Here, we utilized a transplantable version of PYMT model where PYMT tumor cells are inoculated into fourth mammary fat pads of wild-type female C57BL/6 mice. Key experiments were repeated using transgenic MMTV-PYMT mice (FVB background) to determine whether our findings are consistent in distinct model types (transplanted versus spontaneous) and genetic backgrounds (C57BL/6 versus FVB).

We first verified that CDK4/6i palbociclib was effective in a PYMT model. Transplanted PYMT tumors grew slower in palbociclib-treated mice as compared to vehicle-treated animals (Figure 1A). In agreement with cytostatic activity of CDK4/6i (Klein et al., 2018; Knudsen and Witkiewicz, 2017), palbociclib inhibited proliferation of tumor cells based on decreased Ki67 expression (Figures 1B and 1C). Similarly, the growth of spontaneous tumors arising in mammary glands of PYMT-FVB transgenic mice was attenuated by palbociclib (Figure S1A). Final tumor burden determined as combined weight of all tumor lesions per mouse was reduced in the palbociclib group (Figure S1B).

Flow cytometry immunophenotyping was done to determine the effect of CDK4/6i treatment on the composition of tumor immune microenvironment. To assess the temporal variations of the CDK4/6i influence on immune profiles, as well as the effect of tumor size, tumors were analyzed at early (8 days, comparable size in the vehicle and CDK4/6i groups) and late (25 days, reduced size in the CDK4/6i group) time points (arrows on Figure 1A indicate time points of tumor collection). Complete results are shown in Table S1. The percentages of T cells were significantly increased ($p = 0.002$) in tumors from CDK4/6i-treated mice as compared to the vehicle group (Figures 1D and 1E; Table S1) across both time points. There was no significant interaction between treatment effect and day effect on T cell levels suggesting that CDK4/6i-mediated increase of T cells was consistent across tested time points and was not directly influenced by tumor size. Among T cells, $CD8^+$ T cells accumulated in CDK4/6i-treated tumors (Figures 1D and 1E; Table S1). We also detected an increase of B cells after palbociclib treatment; however, the overall levels of B cells were low. Several immune populations were differentially affected at early and late analysis time points,

Figure 1. CDK4/6i treatment increases the number and activity of T cells in mouse model of breast cancer

(A) Growth of PYMT tumors in female C57BL/6 mice treated twice daily with 100 mg/kg CDK4/6i palbociclib or vehicle (n = 20 mice/group, 10 mice/group sacrificed at day 8, mixed-model statistics, data are represented as mean ± SEM). Arrows indicate days of tumor collection for immunophenotyping.

(B) Ki67 IHC staining in tumors from mice treated as in (A).

(C) Quantified percentages on $Ki67^+$ cells in tumors from mice treated as in (A) (n = 3–5 individual tumors, t test, data are presented as individual values and mean ± SD).

(D) Representative plots from flow cytometry analysis of tumor-infiltrating immune cells from mice shown in (A). Tumors were collected at day 8 and 25. Cells were gated on live $CD45^+$ cells.

(E) Percentages of $CD3^+$ and $CD8^+$ cells in tumors from mice shown in (A) (n = 6–9 tumors/group, two-way ANOVA).

(F) Representative plots from flow cytometry analysis of phenotypes of tumor-infiltrating T cells from mice treated twice daily with vehicle or 100 mg/kg palbociclib for 10 days.

(G–I) Percentages on $CD69^+$ (G), $CD137^+$ (H), and $CD134^+$ (I) CD8 T cells from the experiment shown in (F) (n = 5–6 tumors/group, t test). Cells were gated on live/$CD45^+$/$CD3^+$/$CD8^+$ population.

(J) Percentages of tumor-infiltrating Treg cells from the experiment in (F) (n = 5–6 tumors/group, t test). Cells were gated on live/$CD45^+$/$CD3^+$/$CD4^+$ population.

(K) CD8/Treg cell ratios from the experiment shown in (F) (n = 5–6 tumors/group, t test).

(E–K) Data are presented as individual values and mean.

(L–N) Female C57BL/6 mice bearing PYMT tumors were treated twice daily with vehicle or 100 mg/kg CDK4/6i palbociclib. Mice were injected IP with 100 μg of CD8-depleting or isotype control antibodies on day 2 post-palbociclib treatment initiation and every 2 days thereafter. Tumors were collected at day 10. There were 6 mice (12 tumors) in each treatment group.

(L) Representative plots of flow cytometry analysis of $CD8^+$ and $CD4^+$ T cells in blood. Cells were gated on live/$CD45^+$/$CD3^+$ population.

(M) Percentages of $CD8^+$ cells of total $CD3^+$ T cells in blood (n = 4–5 mice/group, t test with Holm-Sidak correction, data are presented as individual values and mean ± SD).

(N) Tumor growth over time (n = 12 tumors/group, mixed model, data are represented as mean ± SEM).

See also Figures S1 and S2 and Table S1.

which may reflect the role of time and size in shaping of tumor immune landscape. For instance, the percentages of NK and NKT significantly decreased from early to late time point; however, they were not significantly affected by palbociclib. There were also cell populations that were affected by palbociclib more prominently as the time went by (treatment and day interaction), such as tumor-associated macrophages, that were not dramatically different at day 8, but were reduced at day 25 (Table S1).

The increase of tumor-infiltrating T cells, and, specifically, $CD8^+$ T cells, by CDK4/6i treatment was also detected in spontaneous tumors from transgenic PYMT FVB mice (Figure S1C), indicating that the effect of CDK4/6i on T cells in consistent in distinct models and genetic backgrounds. Notably, T cells were infiltrating throughout the tumor in both injected (Figure S2A) and spontaneous (Figure S1D) models. The density of T cells varied across tumor sections, with ''hot'' T cell-dense areas present in some of the tested sections of CDK4/6i-treated tumors (Figure S2A; Figure S1D).

We also characterized the effect of CDK4/6i on phenotype of tumor-infiltrating T cells using spectral cytometry. A higher fraction of tumor-infiltrating $CD8^+$ T cells expressed activation marker CD69 in CDK4/6i-treated mice as compared to the vehicle cohort (Figures 1F and 1G). Furthermore, an increase in the percentages of $CD8^+$ T cells expressing co-stimulatory receptors CD137 (4-1BB) and CD134 (OX40) was observed after CDK4/6i treatment (Figures 1F, 1H, and 1I). CDK4/6i decreased the percentages of CD4 T cells expressing markers of T regulatory (Treg) cells, such as $FoxP3^+$ and $FoxP3^+/CD25^+$ (Figures 1F and 1J). Consequently, the CD8/Treg ratio was increased by CDK4/6i treatment (Figure 1K). These data indicate that the T cell infiltrate in CDK4/6i-treated tumors displays more prominent anti-tumor phenotype compared to the vehicle cohort. Dimension reduction analysis using tSNE showed a decrease of the Treg cell cluster and an increase of active $CD8^+$ T cell cluster characterized by high expression of CD69, CD137, and CD134 in CDK4/6i-treated tumors as compared to controls (Figure S2B).

Of note, while PD-L1 expression on myeloid cells was not significantly affected by CDK4/6i treatment (Table S1), we observed an increase in the percentages of PD-L1 expressing CD45-negative tumor cells from 1.3% in the vehicle group to 2.7% in the CDK4/6i treatment group (Figure S2C, $p = 0.005$). Moreover, two out of six tumors in the CDK4/6i treatment group had a proportion of CD45-negative tumor cells that lost MHCI expression (Figure S2D). This effect may indicate compensatory feedback response to increased T cell infiltrate in CDK4/6i-treated tumors.

We next tested whether $CD8^+$ T cells contributed to the overall anti-tumor activity of CDK4/6i. PYMT tumor bearing mice were treated with CDK4/6i or vehicle while also receiving injections of CD8-depleting or isotype control antibody. Levels of peripheral CD8 T cells were prominently reduced by anti-CD8 treatment (Figures 1L and 1M). CDK4/6i inhibited tumor growth in both control and $CD8^+$-depleted mice. However, tumor volumes were smaller in CDK4/6i-treated mice that received isotype control antibodies as compared to CD8-depleted mice (Figure 1N). These data suggest that anti-tumor activity of CDK4/6i was partially dependent on CD8 T cells.

CDK4/6i treatment augments T cell-based therapies

We next tested whether increased levels of activated T cells in CDK4/6i-treated tumors can be harnessed for cancer immunotherapy. Based on the increased expression of co-stimulatory receptors OX40 and 4-1BB on T cells from CDK4/6i-treated tumors, we hypothesized that CDK4/6i will sensitize tumors to antibodies that activate these receptors. Of note, agonistic OX-40 and 4-1BB antibodies are currently in clinical development (ClinicalTrials.gov: NCT03364348 and NCT03217747). Mice inoculated with PYMT cells were treated with vehicle or palbociclib in the presence or absence of mouse-specific OX-40 and 4-1BB agonistic antibodies. No significant inhibition of tumor growth was evident after OX40/4-1BB stimulation in vehicle-treated mice. In contrast, combining palbociclib with OX40/4-1BB stimulation further reduced tumor growth as compared to the palbociclib-only or vehicle treatment cohorts (Figure 2A). Mice treated with palbociclib and anti-OX40/4-1BB displayed the lowest final tumor weight at sacrifice (Figure 2B). We also tested whether combined palbociclib and anti-OX40/4-1BB therapy provided protection from tumor re-growth. PYMT-bearing mice were treated with palbociclib and OX-40/4-1BB antibodies for 25 days and monitored until their tumors reached the end point size (15 mm in diameter) or became perforated. The fraction of surviving mice was numerically higher in palbociclib and the anti-OX40/4-1BB combination treatment cohort; however, the differences were not statistically significant ($p = 0.098$) (Figure 2C). Based on these data, we concluded that combining palbociclib and endogenous T cell stimulation provides a modest improvement of anti-tumor effect over single-agent palbociclib.

We next evaluated whether CDK4/6i can augment anti-tumor activity of adoptive cell therapy (ACT). The OT-1-OVA model was used to recapitulate ACT conditions. PYMT tumor cells engineered to express model antigen OVA were injected into female C57BL/6 mice. When tumors formed, mice were treated with vehicle or palbociclib for 2 weeks and then received injections of OVA-specific T cells derived from spleens and lymph nodes of OT-1 mice and activated *ex vivo* by CD3/CD28 stimulation (Figure 2D). We first tested the recruitment of transferred T cells into vehicle and CDK4/6i-treated tumors. OT-1 T cells were fluorescently tagged prior to injection into mice to distinguish them from endogenous T cells. Tumors were analyzed 2 h post-injection (Figure 2D). We found that tumors from CDK4/6i-treated mice recruited more T cells as compared to tumors in vehicle-treated mice (Figure 2E). This suggests that CDK4/6i promotes recruitment of transferred T cells into the tumor.

We next investigated the impact of CDK4/6i on ACT efficacy. Palbociclib and vehicle pre-treated mice that received either mock injection or activated OT-1 T cells were monitored until their tumors reached end-point size or became perforated. Based on the first time point after T cell administration, palbociclib-treated mice that received mock injection had smaller tumors that accelerated immediately after treatment discontinuation. In contrast, tumors from palbociclib-treated mice that received OT-1 T cells remained slow growing (Figure 2F). As a result, mice in the combination treatment group exhibited improved survival as compared to control vehicle-treated mice

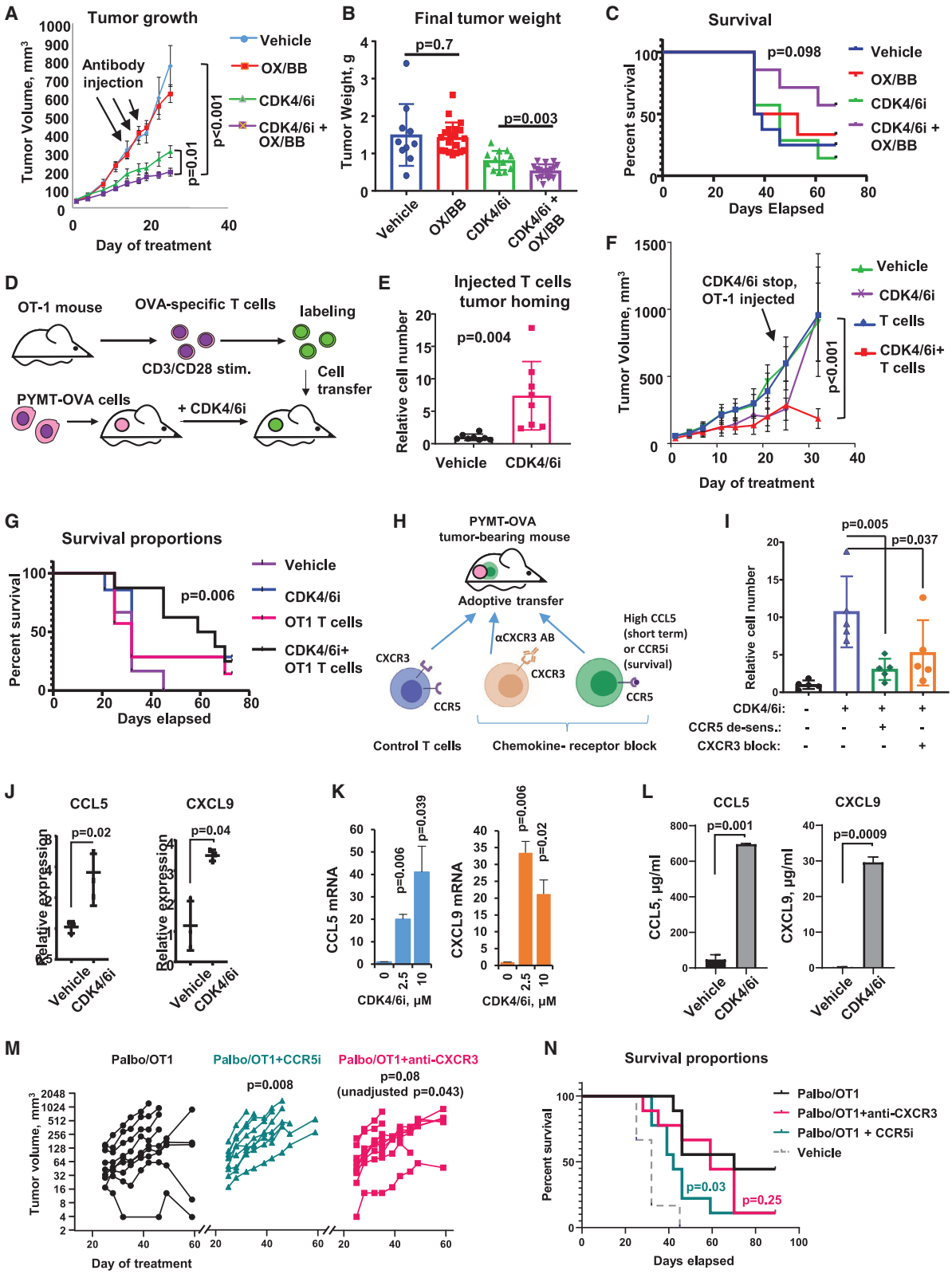

(legend on next page)

(Figure 2G, cf. black and purple lines). No significant survival benefit was observed in the OT-1-only or CDK4/6i-only treatment groups (Figure 2G). These data indicate that CDK4/6i pre-treatment improved recruitment of exogenous T cells into the tumor and augmented the outcome of ACT.

Chemokine receptors CCR5 and CXCR3 facilitate CDK4/6i-mediated T cell recruitment

Immune cell trafficking and localization are regulated by chemokine-chemokine receptor interactions. Activated T cells express chemokine receptors CCR5 and CXCR3 that recognize chemokines CCL5 and CXCL9, 10, and 11, respectively, secreted at the sites of inflammation (Griffith et al., 2014). Therefore, we investigated whether CCR5 and CXCR3 facilitated recruitment of T cells into CDK4/6i-treated tumors by disabling these chemokine receptors on T cells prior to injection. Neutralizing antibody was used to block CXCR3. Incubation with high doses of CCL5 was used to inactivate CCR5. The latter causes internalization of CCR5 that persists for at least 4 h after ligand withdrawal (Escola et al., 2010). T cells were fluorescently labeled and transferred into vehicle and CDK4/6i-treated C57BL/6 mice bearing PYMT-OVA tumors (Figure 2H). Both CCL5 de-sensitization and CXCR3 blockade abrogated homing of transferred T cells into CDK4/6i-treated tumors (Figure 2I).

Based on these findings, we next asked whether CDK4/6i treatment increased the levels of CCR5 and CXCR3 ligands at the tumor site. Indeed, we found that tumors in CDK4/6i-treated mice expressed higher levels of CCR5 ligand CCL5 and CXCR3 ligand CXCL9 as compared to controls (Figure 2J). To determine whether malignant cells, rather than other cell types found within the TME, upregulated chemokines in response to CDK4/6i, we treated PYMT tumors cells with CDK4/6i palbociclib or vehicle *in vitro*. CDK4/6i treatment upregulated CCL5 and CXCL9 in PYMT cells on mRNA level (Figure 2K) and increased their secretion into the culture medium (Figure 2L). These data suggest that CDK4/6i treatment promoted secretion of inflammatory chemokines by tumor cells resulting in improved CCR5 and CXCR3-mediated homing of T cells into the tumor.

To determine whether chemokine-chemokine receptor interactions played a role in CDK4/6i-mediated improvement of ACT outcome, we administered OT-1 T cells to PYMT-OVA tumor-bearing mice. Mice were pre-treated with CDK4/6i for 3 weeks (Figures 2F and 2G) and received treatments blocking CCR5 and CXCR3-mediated trafficking. To block CCR5-CCL5 interaction, maraviroc was used, which is a small-molecule antagonist of CCR5 (CCR5i). To inhibit CXCR3 function, CXCR3-neutralizing antibody was administered *in vivo*. Control mice received CDK4/6i and ACT only. Tumors in mice receiving chemokine receptor blockade exhibited upward growth patterns, while several tumors in the control cohort decreased or stabilized after ACT administration. The overall growth was significantly accelerated in maraviroc-treated mice ($p = 0.008$,

Figure 2. CDK4/6i improves immunotherapy response and promotes chemokine-mediated T cell tumor homing

(A) Tumor growth in C57BL/6 mice implanted with OVA-expressing PYMT tumor cells and treated with CDK4/6i palbociclib (100 mg/kg, twice a day), mix of agonistic antibodies for OX-40 and 4-1BB (OX/BB, 100 μg each per mouse, once every 3 days), a combination of both treatments, or vehicles for 25 days (n = 8–10 mice, two tumors per mouse, mixed-model statistics, data are represented as mean ± SEM).

(B) Final weight of tumors from experiment shown in (A) (n = 10–20 tumors, one-way ANOVA, data are presented as individual values and mean ± SD).

(C) Survival analysis in C57BL/6 mice implanted with OVA-expressing PYMT mammary tumor cells and treated as in (A) for 25 days and then followed till day 68 (n = 10 mice/group, Gehan-Breslow-Wilcoxon test).

(D) Schematic of T cell recruitment experiment. OVA-expressing PYMT cells were implanted in fourth mammary fat pad on female C57BL/6 mice. Mice were treated once a day with 100 mg/kg palbociclib or vehicle for 2 weeks and then received an intravenous (i.v.) injection of OVA-specific T cells. T cells derived from OT-1 mice were activated with anti-CD3/CD28 antibodies and fluorescently labeled *ex vivo*. Tumors were collected 2 h after cell transfer.

(E) Numbers of labeled T cells in tumors of C57BL/6 mice from experiment described in (D) (n = 8 tumors/group, t test, data are presented as individual values and mean ± SD).

(F) Tumor growth in C57BL/6 mice implanted with OVA-expressing PYMT mammary tumor cells and treated once a day with 100 mg/kg CDK4/6i palbociclib or vehicle for 3 weeks followed by injection of OT-1 T cells or saline. Mice were followed until tumors reached end point size or became perforated (n = 7 mice/group, mixed model, data are represented as mean ± SEM).

(G) Survival analysis of mice from in (F). OT1 injection was given at day 25 (n = 7, log-rank [Mantel-Cox) statistical comparison between Vehicle and CDK4/6i$^+$OT1 groups is shown). The experiment was repeated with consistent results.

(H) Scheme of an *in vivo* T cell recruitment experiment. C57BL/6 mice were inoculated with PYMT-OVA cells. Mice were treated with vehicle or CDK4/6i palbociclib at 100 mg/kg for 25 days followed by i.v. injection of activated OT-1 T cells. To block CCR5 and CXCR3-mediated migration, OT-1 T cells were treated with high dose of CCL5 or CXCR3-blocking antibody prior to transfer. T cells were labeled with cell tracker prior to injection into mice.

(I) Accumulation of fluorescent transferred T cells in PYMT tumors from experiment described in (L) (n = 5 mice/group, one-way ANOVA, data are presented as individual values and mean ± SD).

(J) Real-time PCR analysis of CCL5 and CXCL10 mRNA in PYMT tumors from mice treated as in (A) (n = 3 tumors, t test after log transformation, data are presented as individual values and mean ± SD).

(K) CCL5 and CXCL9 mRNA expression in PYMT tumor cells treated with vehicle or CDK4/6i (palbociclib, 1 μM) for 3 days *in vitro* (n = 2, t test, data are represented as mean ± SD).

(L) ELISA analysis of indicated chemokines in the conditioned medium of PYMT cells treated with vehicle or 1 μm palbociclib for 5 days (n = 2, t test, data are represented as mean ± SD).

(M) Tumor volume change overtime with and without chemokine receptor blockade. Female C57BL/6 mice were implanted with PYMT-OVA tumors and treated with palbociclib for 25 days and injected with activated OT-1 T cells (treatment scheduler was same as in F). A subgroup of mice received CCR5i maraviroc (10 mg/kg, once daily oral gavage) or CXCR3-blocking antibody (200 μM per mouse, i.v. injection every 3 days) on days 25–42. Mixed model with Dunnett's post-test was used for statistical comparison of tumor growth between the control CDK4/6i$^+$OT-1 group and chemokine-receptor-inhibited groups (n = 9 mice per group, individual data presented). p value with and without adjustment for multiple comparison is shown for the CXCR3-blockade group.

(N) Survival curves from experiment in (M) (n = 9, log-rank (Mantel-Cox) statistical comparison between the CDK4/6i$^+$OT1 and chemokine-receptor inhibited groups).

CellPress
OPEN ACCESS

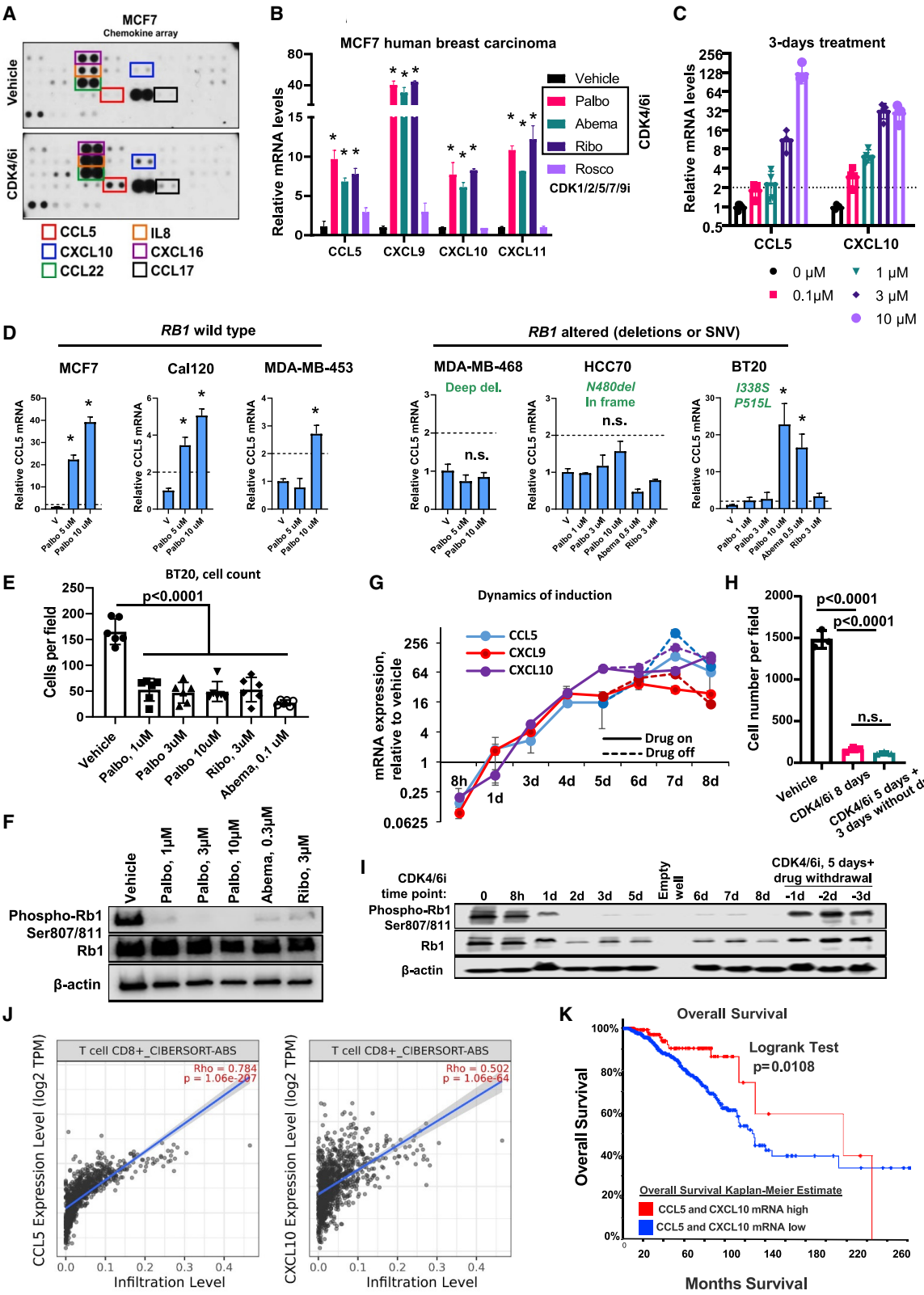

(legend on next page)

Figure 2M). CXCR3-inhibited mice exhibited similar trend; however, after adjusting the p value for multiple comparisons, the effect was not significant (adj. p = 0.08., raw p = 0.043, Figure 2M). Notably, CCL5i-co-treated mice exhibited worse survival in comparison to control (chemokine receptor-functional) mice (Figure 2N). The effect of anti-CXCR3-treatement on survival was not significant. Of note, 4 out of 9 mice survived over 90 days after ACT administration in the control group, as compared to 1 out 9 mice in the chemokine receptor-inhibited groups (Figure 2N). These data suggest that CDK4/6i-mediated improvement of ACT efficacy is, at least in part, dependent on chemokine receptors, especially CCR5.

CDK4/6i-treated human breast cancer cells produce T cell-recruiting chemokines

We next investigated whether our mouse model findings were relevant to human breast cancer. To test whether CDK4/6i induced inflammatory chemokines in the human model, ER^+ breast cancer cells MCF7 were treated with CDK4/6i or vehicle control, and the levels of secreted chemokines were measured in the conditioned media using a chemokine array. Several chemokines were upregulated in CDK4/6i-treated cells, including CCR5 ligand CCL5 and CXCR3 ligand CXCL10 (Figure 3A). Increased chemokine secretion was associated with increased expression of chemokine mRNA indicating upregulation on a transcriptional level (Figure 3B). Similar to CXCL10, expression of two other CXCR3 ligands, CXCL9 and CXCL11, was increased after palbociclib treatment. We confirmed that two other structurally distinct CDK4/6 inhibitors, ribociclib and abemaciclib, also upregulated chemokines in human breast cancer cells. In contrast, treatment with roscovitin that inhibits CDK1/2/5/7/9, but not CDK4 or CDK6, showed minimal effect on chemokine expression (Figure 3B). This suggests that chemokine induction is an ''on-target'' effect of CDK4/6 inhibition. Chemokine induction was dose dependent at the 3-day treatment time point with the level of induction increasing progressively within the 0.1–10 μM range of palbociclib concentrations (Figure 3C). Treatment was not toxic at these conditions based on propidium iodide cytotoxicity assay (Figures S3A and S3B).

Inactivating mutations/deletions of *RB1* gene are associated with CDK4/6i resistance (Álvarez-Fernández and Malumbres, 2020). Therefore, we tested whether chemokine induction by palbociclib was linked with *RB1* status. We tested the induction of CCL5 by palbociclib in a panel of cell lines with wild-type and deleted/mutated *RB1.* Information on *RB1*status was obtained from cBIO portal (Cancer Cell Line Encyclopedia [CCLE] dataset) (Cerami et al., 2012). Two- or greater fold induction of CCL5 was detected in three tested *RB1* wild-type lines: MCF7, Cal120, and MDA-MB-453 (Figure 3D). Two out of three *RB1*-altered lines showed no significant CCL5 induction after CDK4/6i treatment. Surprisingly, BT20 cells that have two amino acid substitutions in RB1 protein, I338S and P515L, exhibited strong induction of CCL5 mRNA after treatment with palbociclib. This induction was likely on target because another CDK4/6i abemaciclib also induced CCL5 in BT20 cells (Figure 3D, right panel). To investigate this paradoxical activity further, we tested whether BT20 responded to CDK4/6i. Indeed, we found that cell numbers were reduced in cultures of BT20 cells treated with different CDK4/6 inhibitors as compared to vehicle-treated cells (Figure 3E). Furthermore, western blot analysis indicated reduction of the CDK4/6-mediated inhibitory RB1 phosphorylation by CDK4/6i treatment (Figure 3F). Based on these data, it is likely that the specific *RB1* genetic alterations found in BT20 cells were not strongly detrimental to RB protein function, which is why these cells responded to CDK4/6i. This conclusion is consistent with data from other groups showing that BT20 cells are responsive to palbociclib (Finn et al., 2009). Collectively, these data suggest that CDK4/6i-mediated chemokine induction is linked with RB inhibition.

Figure 3. CDK4/6i-treated breast cancer cells secrete chemokines associated with T cell infiltrate and favorable prognosis in breast cancer patients

(A) Results of the cytokine array in conditioned media from MCF7 cells treated for 4 days with 1 μM palbociclib or vehicle control. Proteins elevated after palbociclib (CDK4/6i) treatment are indicated with frames.

(B) Real-time PCR detection of CCL5, CXCL9, 10, 11 mRNA in MCF7 cells treated with 1 μM palbociclib, 3 μM ribociclib, 0.2 μM abemaciclib for 4 days. As a non-CDK4/6i control, cells were treated with 10 μM roscovitin (n = 3, t test, data are represented as mean ± SD, *p < 0.05).

(C) Results of the real-time PCR analysis of CCL5, CXCL9, and CXCL10 mRNA in MCF7 cells treated with palbociclib for 3 days at indicated concentrations (n = 3, t test, *p < 0.05, data are presented as individual values, mean ± SD).

(D) Real-time PCR analysis of CCL5 mRNA induction by palbociclib in six indicated cells lines with wild-type or altered *RB1* gene (n = 2–3, one-way ANOVA, (n = 3, t test, data are represented as mean ± SD, *p < 0.05).

(E) Numbers of BT20 cells after 5 days of treatment with indicated CDK4/6 inhibitors or vehicle. Cells were stained with crystal violet and imaged in transmitted light (n = 6, one-way ANOVA, data are presented as individual values and mean ± SD).

(F) Western blot analysis of the inhibition of RB1 hyper-phosphorylation in BT20 cells treated as described in (E).

(G) Real-time PCR detection of CCL5, CXCL9, and CXCL10 in MCF7 cells treated with 1 μM palbociclib. Samples were collected at indicated time points ranging from 8 h to 8 days. Solid lines represent samples that were continuously treated with palbociclib. Punctate lines indicate samples where palbociclib was removed from culture media after day 5 of treatment.

(H) Numbers of crystal violet stained MCF7 cells treated as described in (G). Cells were treated with 1 μM palbociclib for 8 days continuously or treated for 5 days followed by drug washout and an additional 3 days of culture without drug. Control cells were treated with vehicle for 8 days (n = 3, one-way ANOVA, data are presented as individual values and mean ± SD).

(I) Western blot analysis of RB phosphorylation in MCF7 cells treated as described in (G).

(J) Correlation of CCL5 (right panel) or CXCL10 (left panel) mRNA with $CD8^+$ T cell infiltrate computed by CIBERSORT in TCGA set of luminal A breast cancer tumors (N = 1,100).

(K) Comparison of overall survival in breast cancer patients with high expression of either CCL5, CXCL10, or both in their tumors (*Z* score > +1 [median ± 1 SD]) as compared to the rest of the cases in TCGA breast cancer dataset (N = 1,093, log-rank test).

See also Figures S3 and S4.

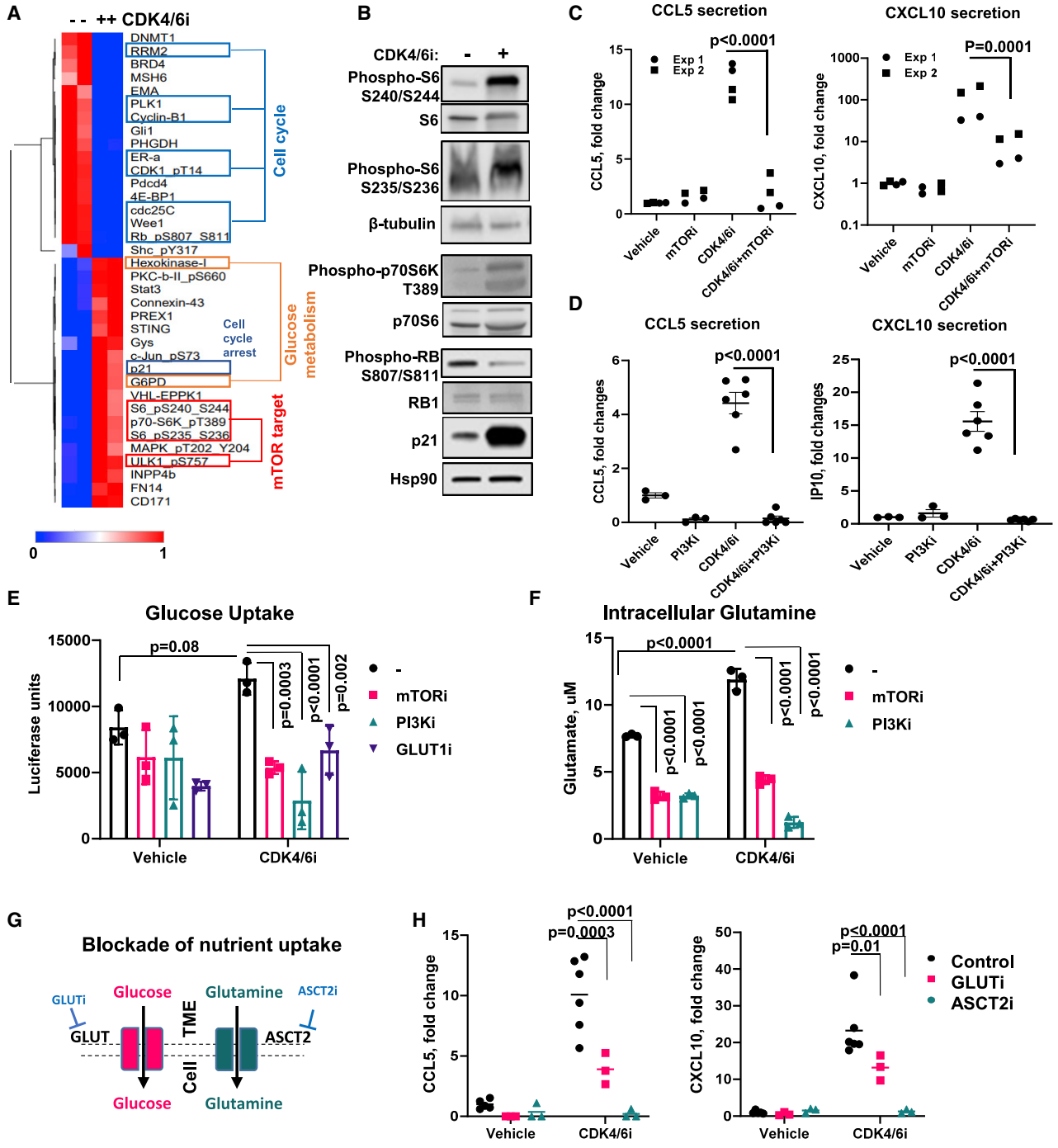

Figure 4. mTOR-regulated metabolic activity is required for CDK4/6i-mediated chemokine induction

(A) RPPA proteomic profiling of MCF7 cells treated with vehicle or 5 μM CDK4/6i (Palbociclib) for 5 days. The heatmap shows proteins that passed the 1.5-fold change and $p < 0.05$ (multiple t test) cutoff.

(B) Western blot validation of RPPA data.

(C) ELISA measurements of CL5 and CXCL10 in the conditioned medium of MCF7 cells treated with vehicle or 5 μM palbociclib ± 2 μM mTORi rapamycin for 5 days (n = 4 biological replicates pooled from 2 independent experiments, two-way ANOVA, individual data presented).

(D) ELISA measurements of CCL5 and CXCL10 in the conditioned medium of MCF7 cells treated with vehicle or 5 μM palbociclib ± 0.5 μM PI3Ki BKM120 (buparlisib) for 5 days (n = 3-6 biological replicates, one-way ANOVA, data are presented as individual values, mean ± SEM).

(E) Results of the luciferase-based glucose uptake assay in MCF7 cells treated with vehicle or 1 μM CDK4/6i palbociclib ± 2 μM mTORi rapamycin, or 0.5 μM of PI3Ki BKM120 (buparlisib) for 5 days (n = 3 biological replicates, one-way ANOVA, data are presented as individual values and mean ± SD).

(legend continued on next page)

We also showed that the induction of CCL5 and CXCL9/10 in response to CDK4/6i treatment was time dependent. The levels of induction increased over time reaching a plateau around day 5 of continuous treatment (Figure 3G). Notably, cells that were treated with palbociclib for 5 days continued to produce high levels of chemokines when drug was removed from the culture media (Figure 3G, punctate lines). The numbers of cells were comparable after "5 days on $^{+}$ 3 days off" and "8 days on" treatments (Figure 3H), suggesting that palbociclib-induced cell cycle arrest was not immediately reversible. In agreement with this conclusion, we detected an increased percentage of cells positive for senescence-associated β galactosidase (SA-βGal) after 5 days of CDK4/6i treatment (Figures S4A and S4B), which is a marker of cellular senescence. Senescence is a type of persistent growth arrest that occurs in response to a variety of damaging conditions and is associated with increased secretion of many factors, including pro-inflammatory chemokines CCL5 and CXCL9,10,11 (Vilgelm et al., 2019). In contrast to cell cycle arrest, the levels of inhibitory RB1 phosphorylation showed full recovery to the baseline levels after palbociclib withdrawal, indicating reactivation of CDK4 and CDK6 (Figure 3I). Altogether these data suggest that, although the effect of palbociclib on CDK4/6 activity was reversible, the damage done to the cell during the 5-day treatment was not. Since chemokine expression was also not reversible, we concluded that chemokine induction was not directly dependent in CDK4/6 activity but rather was associated with cell damage induced by CDK4/6i treatment.

Chemokine expression is a favorable prognostic factor in breast cancer patients

Our results showed that CDK4/6i induced chemokines in breast cancer cells. Therefore, we sought to understand how elevated chemokine expression may impact patients with breast cancer. TIMER2.0 analysis of a TCGA dataset that included over a thousand luminal A breast cancer samples (Li et al., 2020) demonstrated strong association of CCL5 and CXCL10 expression with CD8 T cell infiltrate estimated by CIBERSORT algorithm (Figure 3J). Furthermore, breast cancer patients with elevated expression of CCL5 and CXCL10 in their tumors (defined by a *Z* score threshold of ±1 SD) exhibited improved overall survival in comparison to patients with low-to-moderate chemokine expression (Figure 3K). These data suggest that increased chemokine expression in CDK4/6i-treated tumors can have beneficial effect on patients' outcome.

CDK4/6i inhibits expression of cell cycle mediators while promoting mTOR activity

We next investigated the mechanism of CDK4/6-mediated chemokine induction. Palbociclib- and vehicle-treated MCF7 cells were subjected to reverse phase protein array (RPPA) analysis that detects expression of 471 proteins and phosphoproteins. Proteins that were significantly up- or downregulated after CDK4/6i treatment are presented on a heatmap (Figure 4A). Compete RPPA data are provided in Table S2. As expected, we observed downregulation of proliferation-related proteins (phosphorylated RB, cyclin B1, Wee1, PLK1, etc.) along with upregulation of cell cycle arrest inducer p21 in CDK4/6i-treated cells (Figure 4A, blue frames). One pattern that caught our attention was the increased phosphorylation of mTOR kinase targets, such as S6, p70-S6K, and ULK1 in CDK4/6i-treated cells (Figure 4A, red frames). Western blot analysis confirmed increased phosphorylation of S6 on residues S240-244, and S235-236, and 70-S6K on T389 after CDK4/6i treatment (Figure 4B). These changes are indicative of the mammalian target of rapamycin complex 1 (mTORC1) activity (Liu and Sabatini, 2020).

A number of prior studies showed the requirement of mTOR for chemokine induction in some immune cell subsets, such as monocytes and macrophages (Jin and Zhao, 2020; Lin et al., 2014; William et al., 2019). Therefore, we investigated whether mTOR was similarly involved in chemokine induction in breast cancer cells treated with CDK4/6i. MCF7 cells were treated with vehicle or palbociclib in the presence or absence of mTOR inhibitor rapamycin. We found that CDK4/6i-induced secretion of CCL5 and CXCL10 was abrogated in the presence of mTOR inhibitor, suggesting that mTOR activity was necessary for chemokine induction (Figure 4C). Similarly, inhibition of upstream mTOR activator PI3K (Laplante and Sabatini, 2012) with a small-molecule inhibitor BKM120 (buparlisib) abolished chemokine induction by CDK4/6i (Figure 4D). In agreement with these experimental findings, cBIO analysis of the TCGA dataset of 960 breast carcinoma specimens showed higher content of mTOR activity marker phosphorylated S6 protein (residues S235/S236 and S240/S244) in tumors with elevated CCL5 and CXCL10 expression (Figure S5A).

Prior studies indicated that targeting PI3K/mTOR pathway in the context of CDK4/6i treatment could improve tumor growth inhibition and prevent acquisition of resistance via tumor intrinsic mechanisms (O'Brien et al., 2020; Vilgelm et al., 2019; Yoshida et al., 2019). However, these preclinical studies used immunodeficient mice lacking T cells. Here, we tested how combined CDK4/6 and mTOR inhibition affects tumor growth and immune infiltrate in immunocompetent model. Female C57BL/6 mice were injected with PYMT tumor cells and treated with vehicle, CDK4/6i palbociclib, mTOR inhibitor everolimus (currently used for treatment of human breast cancer), or a combination of both drugs (Figure S5B). Tumor growth was most prominently inhibited in the CDK4/6i and mTORi combination group. There was a significant benefit of combining CDK4/6i with mTORi over CDK4/6i single agent ($p = 0.048$) but not over single-agent mTORi ($p = 0.094$). Flow cytometry analysis indicated a decrease of $CD3^{+}$ T cells, including $CD8^{+}$ T cells, in the CDK4/6i and mTORi combination group as compared to CDK4/6i single agent

(F) Same as (E) except intracellular glutamate was measured.
(G) Schematic of the experimental approach to block glucose and glutamine uptake for the experiment in (H).
(H) ELISA measurements of CCL5 and CXCL10 in the conditioned media from MCF cells treated for 5 days with 5 μM CDK4/6i palbociclib in the presence or absence of pharmacological inhibitors of glucose (1 μM Bay876, GLUTi) or glutamine (10 mM O-Benzyl-L-Serine, ASCTi) transporters (n = 3-6 biological replicates, two-way ANOVA, data are presented as individual values and mean).
See also Figure S5 and Table S2.

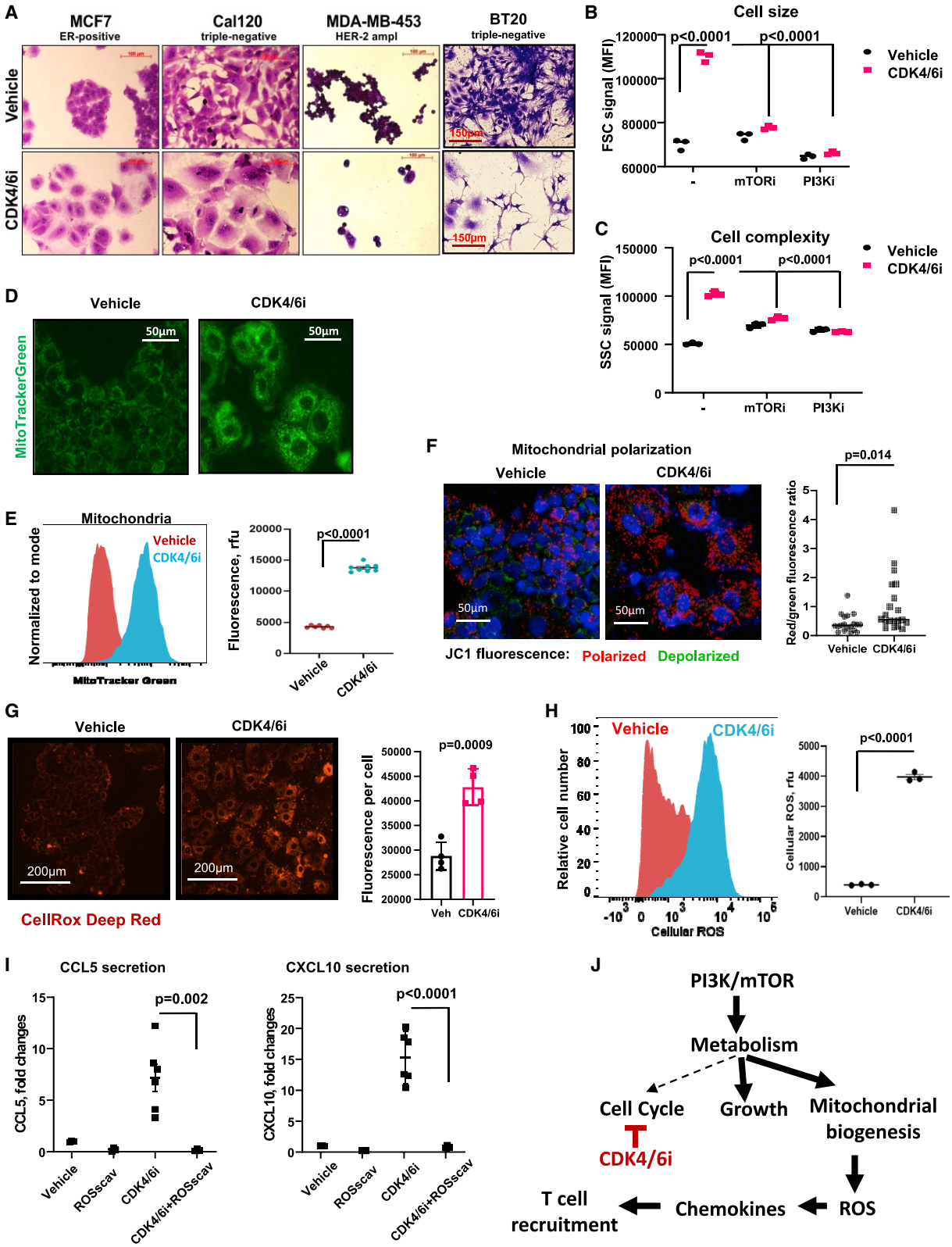

(legend on next page)

(Figure S5C). Considering the critical role of mTOR in immune system function (Weichhart et al., 2015), the mechanism of tumor immunome modulation by the mTORi is likely complex. Thus, while our results are in agreement with mTOR being a promising co-target in the context of CDK4/6i treatment, they also indicate that mTORi co-targeting may not be advisable in situations when T cell-enriched microenvironment is desired (i.e., if immunotherapy is planned). Dedicated future studies will be required to address the complex role of mTOR in anti-tumor immunity.

mTOR-regulated metabolic activity is required for CDK4/6i-mediated chemokine induction

We next sought to determine how mTOR regulated chemokine expression in CDK4/6i-treated cells. mTOR is a central regulator of cell metabolism (Sabatini, 2017; Saxton and Sabatini, 2017). Therefore, we investigated whether CDK4/6i-treated cells were metabolically active. RPPA indicated upregulation of a number of metabolism-associate proteins in CDK4/6i-treated cells including hexokinase I (HK1), glycogen synthase (Gys), and glucose-6-phospate dehydrogenase (G6PD) (Figure 4A, orange frames). However, some metabolic proteins were differentially affected by CDK4/6i. For instance, a mediator of serine metabolism PHGDH was downregulated by palbociclib (Figure 4A).

To further investigate the effect of CDK4/6i on cell metabolic activity, we measured glucose uptake and glutamine utilization in vehicle and palbociclib-treated MCF7 cells. Glucose and glutamine are critical nutrients required for cancer cell growth and their consumption reflects cell's metabolic demands. Notably, CDK4/6i treatment did not inhibit nutrient consumption (Figures 4D and 4E). In fact, the levels of intracellular glutamate, a product of glutamine conversion within the cells, was increased in CDK4/6i-treated cells as compared to vehicle-treated cells (Figure 4E). Furthermore, inhibition of mTOR or its upstream regulator PI3K down-modulated glucose uptake and glutamine utilization in CDK4/6i-treated cells. These data suggest that mTOR is required to maintain metabolic activity in CDK4/6i-treated cells. To test whether maintenance of high metabolic activity played role in CDK4/6-mediated chemokine induction, we blocked nutrient uptake in breast cancer cells using pharmacological inhibitors of glucose transporter GLUT (GLUTi Bay876) or glutamine transporter ASCT2 (and O-benzyl-L-serine, respectively) (Figure 4F). Both inhibitors abrogated CCL5 and CXCL10 induction after CDK4/6i treatment (Figure 4G).

CDK4/6i-mediated chemokine production is associated with cell hypertrophy, accumulation of mitochondria, and induction of ROS

Generally, active metabolism and high mTOR activity are characteristics of fast proliferating cells. Indeed, mTOR promotes anabolic metabolism and biosynthesis to coordinate cell division with doubling of cell biomass and organelle biogenesis. Quiescence cells often inactivate the mTOR kinase due to the lack of need for cell growth (Valcourt et al., 2012). Therefore, we were surprised to detect activation of mTOR and metabolism in cells treated with CDK4/6i that inhibits proliferation. Hence, we sought to understand how increased metabolic activity was utilized in CDK4/6i-treated cells. We found that palbociclib treatment caused cell hypertrophy in breast cancer lines (Figure 5A). An increase in cell sizes after palbociclib was confirmed by flow cytometry (Figure 5B). Cell growth phenotype was driven by PI3K/mTOR pathway as pharmacological inhibition of either mTOR or PI3K abrogated CDK4/6i-mediated cell size increase (Figure 5B; Figure S5F). CDK4/6i-treated cells also exhibited an increase of the cell complexity as per flow cytometry analysis, which indicates increased organelle content. Similar to the increased size, increased complexity was alleviated by mTOR and PI3K inhibition (Figure 5C). We next investigated whether mitochondria were among the organelles accumulating in CDK4/6i-treated cells based on mTOR being a key driver of mitochondrial biogenesis (Morita et al., 2013). Indeed, mitochondrial content was increased in cells treated with CDK4/6i based on mitotracker staining detected by microscopy (Figure 5D) and flow cytometry (Figure 5E). To test whether mitochondria were functional in CDK4/6i-treated cells, we used a JC-1 mitochondrial potential probe. JC-1 forms aggregates in healthy polarized mitochondria that emit red fluorescence. Cells with depolarized

Figure 5. CDK4/6i-mediated chemokine production is associated with cell hypertrophy, accumulation of mitochondria, and induction of ROS

(A) Microscopic images of crystal violet stained cells that were treated for 5 days with 5 μM of palbociclib, except for BT20, which were treated with 1 μM palbociclib.

(B) Flow cytometry measurement of forward-scattered light (FCS) parameter indicative of cell volume. MCF7 cells treated with vehicle or 1 μM palbociclib ± 2 μM mTORi rapamycin, or 0.5 μM of PI3Ki BKM120 (buparlisib) for 5 days (n = 3, one-way ANOVA, data are presented as individual values and mean).

(C) Same as (F), except side-scattered light (SSC) channel signals indicative of cell complexity (presence of granules and organelles) are shown.

(D) Fluorescent microscopy of mitochondria detected with MitoTracker Green in MCF7 cells treated with vehicle or 5 μM CDK4/6i palbociclib for 5 days.

(E) Quantification of the MitoTracker staining shown in (D) using flow cytometry (n = 6–8, one-way ANOVA, data are presented as individual values and mean).

(F) Mitochondrial potential analysis using JC-1 biosensor. Red punctate signal, aggregates of JC-1 in polarized mitochondria; green cytoplasmic staining, free JC-1 monomers. Random microscopic fields from 4 biological replicates quantified with ImageJ (n = 19–20, t test, data are presented as individual values and mean).

(G) Representative fluorescence microscopy images of cellular ROS detected with CellROX Deep Red in MCF7 cells treated with vehicle or 5 μM palbociclib (CDK4/6i) for 5 days. Right panel shows average values of ROS fluorescence per cell from 4 biological replicates compared using t test. Data are presented as individual values, mean ± SD.

(H) Representative histogram (left panel) from flow cytometry analysis of cellular ROS in MCF7 cells treated with vehicle or 5 μM CDK4/6i palbociclib for 5 days. Right panel shows quantified data (n = 3, t test, data are presented as individual values, mean ± SEM).

(I) Levels of chemokines CCL5 and CXCL10 in the conditioned media from MCF7 cells treated with 5 mM of cellular ROS scavenger NAC, CDK4/6i (5 μM), combination of both, or vehicle for 5 days (n = 4–6, one-way ANOVA, data are presented as individual values, mean ± SEM).

(J) Proposed model CDK4/6i-mediated chemokine induction. Briefly, the PI3K/mTOR pathway remains active in CDK4/6i-treated cells despite the decreased metabolic demands due to the cell cycle arrest. This leads to exacerbated cell growth and mitochondrial levels and activity associated with oxidative stress, which, in turn, promotes production of T cell-recruiting chemokines.

mitochondria exhibit loss of a red punctate fluorescence and increase of diffuse green fluorescence from JC-1 monomers diffused in the cytoplasm. We detected strong red fluorescence in both vehicle and CDK4/6i-treated cells. Furthermore, red/green ratio was further increased after CDK4/6i treatment indicating high mitochondrial activity (Figure 5F).

Mitochondria are a key source of intracellular ROS (Scialò et al., 2017). Furthermore, CDK4/6i has been shown to induce ROS in pancreatic cancer cells as a result of mTOR-mediated increase of glycolytic and oxidative metabolism and mitochondrial content (Franco et al., 2016), and we observed similar metabolic changes here in a model of breast cancer. Accordingly, we detected increased ROS levels after 5-day palbociclib treatment by fluorescence microscopy (Figure 5G) and flow cytometry (Figure 5H). ROS is a potent pro-inflammatory signal known to induce expression of chemokines and other inflammatory mediators (Sozzani et al., 2005). Therefore, we next evaluated whether ROS was involved in CDK4/6i-induced chemokine secretion. We measured cellular ROS production in MCF7 cells and found it to be increased after 5 days of palbociclib treatment. Removal of ROS using ROS scavenger N-acetylcysteine (NAC) completely abrogated CDK4/6i-mediated chemokine production (Figure 5I). These data suggest that CDK4/6i-mediated chemokine induction in breast cancer cells requires ROS.

Collectively our data suggest that palbociclib inhibited cell cycle arrest without concurrently shutting down cell metabolism. Cells continued to uptake nutrients to supply energy/building blocks for mTOR-driven biosynthesis. The uncoupling of metabolic need and supply manifested in increased cell size and mitochondrial biogenesis and activity associated with accumulation of ROS, which, in turn, induced inflammatory chemokines that recruited T cells into the tumor (Figure 5J).

DISCUSSION

Here, we show that CDK4/6i palbociclib promotes recruitment of T cells into mammary tumors by inducing expression of T cell-chemotactic chemokines in tumor cells. This finding has several clinical implications. First, the ability of CDK4/6i to enhance T cell tumor homing could make these agents useful for sensitizing patients to T cell-delivering therapies such as adoptive cell transfer of T cells and CAR T cells. Indeed, our pre-clinical model showed that CDK4/6i pre-treatment improved outcome and survival of mice that received transfer of activated tumor-specific T cells. Second, TCGA analysis showed that increased expression of chemokines CCL5 and CXCL10, which are induced by CDK4/6i, is an overall positive prognostic factor in breast cancer. Furthermore, recently published expression analysis of breast cancers tumors before and after treatment with CDK4/6i abemaciclib and aromatize inhibitor anastrosole (neoMONARCH study) showed CCL5 induction and overall enrichment of the chemokine/chemokine receptor expression signature after CDK4/6i treatment (Hurvitz et al., 2020), which is in agreement with our mouse model findings.

The present study uncovered the mechanism of CDK4/6i-mediated chemokine induction. We found it to be dependent on metabolic alterations that occurred in cells after CDK4/6i treatment. These changes included activation of mTOR, induction of glucose and glutamine metabolism accompanied by the increase in cell size and mitochondrial/lysosomal content. Metabolic activation after CDK4/6i treatment was reported previously (Warth et al., 2019; Warth et al., 2018; Zanuy et al., 2012). For example, CDK4/6i-treated pancreatic cancer cells exhibited accumulation of ATP, increased mitochondrial mass, activation of glycolytic, and oxidative metabolism driven by the mTOR activation (Franco et al., 2016). Similarly, Cretella et al. (2018) showed that CDK4/6i treatment activated PI3K/AKT/mTOR pathway in TNBC cells, and co-inhibition of this pathway impaired glucose metabolism (Cretella et al., 2018). Inhibition of CDK4/6 with siRNA or specific pharmacologic inhibitor increased glutamine metabolism, mitochondrial content, and mTOR pathway activity in colon cancer cells (Tarrado-Castellarnau et al., 2017). Activation of mTOR was also reported in melanoma PDXs and in patients treated with CDK4/6i (Teh et al., 2018; Vilgelm et al., 2019). Here, we showed that mTOR-mediated metabolic reprogramming was critical for CDK4/6i-mediated chemokine induction. Blockade of metabolism by inhibiting the uptake of two key nutrients consumed by proliferating cancer cells, glucose and glutamine, inhibited CDK4/6i-mediated chemokine production.

Cell cycle machinery and metabolism are interconnected. Proliferating cells display high metabolic activity that ensures availability of metabolites for DNA synthesis and cell growth. This is in contrast to quiescent cells that have low metabolic demands (Valcourt et al., 2012). Surprisingly, despite being in a state of cell cycle arrest, CDK4/6i-treated breast cancer cells displayed phenotype of active metabolism. Thus, we postulated that excessive metabolic activity caused metabolic stress in CDK4/6i-treated cells due to nutrient excess. This could be analogous to chronic organismal over-nutrition (obesity), which can lead to various pathological conditions (Wellen and Thompson, 2010). One of the key markers of metabolic stress induced by nutrient excess is an excessive production of ROS and oxidative stress (Wellen and Thompson, 2010). Accordingly, we found increased ROS content in CDK4/6i-treated cells, which was required for CDK4/6i-mediated chemokine production. Furthermore, CDK4/6i induced mitochondria content and activity, which are the major source intracellular ROS (Gogvadze et al., 2008).

Oxidative stress is a key link between metabolic stress and inflammatory stress response. For instance, ROS has been implicated as a key driver of chronic inflammation in many diseases associated with metabolic dysfunction, including atherosclerosis, diabetes mellitus, and stroke (Forrester et al., 2018). ROS play important role in regulation of inflammatory response associated with activation of pattern recognition receptors, nuclear factor κB (NF-κB), and inflammasome (Forrester et al., 2018; Lugrin et al., 2014). Moreover, ROS are required for normal function of innate and adaptive immune cells, which further underlines their role as a key immune mediator (Chen et al., 2018; Kohchi et al., 2009; Yarosz and Chang, 2018). It is plausible that the biological significance of ROS-mediated induction of chemokines in context of CDK4/6i treatment is to alert the immune system of cell damage. Indeed, excessive ROS can damage cellular DNA leading to mutations that pose risk of oncogenic transformation; therefore, immune recognition of such cells can be beneficial.

Our data highlight an important role of inflammatory chemokines produced by malignant cells in regulation of the composition of tumor immune microenvironment, immunotherapy response, and patient outcome. One can envision T cell recruiting chemokines being useful as prognostic markers for patient stratification for immunotherapy treatment. Furthermore, with the advancement of the circulating tumor cell technology, longitudinal assessment of chemokine expression in tumor cell can be performed. This type of analysis can identify the perfect window for second hit immunotherapy administration in patients treated with CDK4/6i or other agents that induce chemokine expression in tumor cells, such as senescence-inducing drugs and epigenetic modulators (Dangaj et al., 2019; Vilgelm et al., 2015b, 2016). The findings presented here raise a possibility of utilizing CDK4/6 inhibitors to enhance anti-tumor immunity and immunotherapy response in "cold" T cell-excluded tumors.

STAR★METHODS

Detailed methods are provided in the online version of this paper and include the following:

- KEY RESOURCES TABLE
- RESOURCE AVAILABILITY
  - Lead contact
  - Materials availability
  - Data and code availability
- EXPERIMENTAL MODEL AND SUBJECT DETAILS
  - Mice
  - Cell lines
- METHOD DETAILS
  - T cell activation and labeling
  - Chemokine expression analysis
  - Proteomics and western blot
  - Flow cytometry
  - Fluorescence and bright-field microscopy
  - TCGA analysis
- QUANTIFICATION AND STATISTICAL ANALYSIS

SUPPLEMENTAL INFORMATION

Supplemental information can be found online at https://doi.org/10.1016/j.celrep.2021.108944.

ACKNOWLEDGMENTS

This work was supported by grants from BCRF (IIDRP-16-001 to A.E.V.); NCI SPORE in Breast Cancer (P50CA098131) pilot award (to A.E.V.); NIH R37 CA233770-01 (to A.E.V.); the Department of Veterans Affairs (5101BX000196-04 to A.R.); NIH (CA116021 and CA116021-S1 to A.R.); and Senior Research Career Scientist Award (to A.R.). Support for core facilities used in this study was provided by VanderbiltIngram Cancer Center (P30 CA68485). The Reverse Phase Protein Array (RPPA) Core at MD Anderson Cancer Center (The University of Texas) is funded by NCI CA16672.

AUTHOR CONTRIBUTIONS

R.V.U. and A.V. designed experiments. R.V.U., A.E.V., V.B., Z.O., A.B., S.M., N.S., and H.A.L. performed experiments and analyzed data. C.S., S.-C.C., and G.D.A. performed statistical analysis. C.A. and A.R. provided conceptual guidance. C.A., A.R., and D.G.D. provided models/reagents. A.V. supervised the study. R.V.U., A.V., and V.B. wrote the manuscript and prepared figures and tables. All authors reviewed and edited the manuscript.

DECLARATION OF INTERESTS

The authors declare no competing interests.

Received: May 28, 2020
Revised: January 8, 2021
Accepted: March 15, 2021
Published: April 6, 2021

REFERENCES

Álvarez-Fernández, M., and Malumbres, M. (2020). Mechanisms of Sensitivity and Resistance to CDK4/6 Inhibition. Cancer Cell *37*, 514–529.

Ayers, M., Lunceford, J., Nebozhyn, M., Murphy, E., Loboda, A., Kaufman, D.R., Albright, A., Cheng, J.D., Kang, S.P., Shankaran, V., et al. (2017). IFN-γ-related mRNA profile predicts clinical response to PD-1 blockade. J. Clin. Invest. *127*, 2930–2940.

Böttcher, J.P., Bonavita, E., Chakravarty, P., Blees, H., Cabeza-Cabrerizo, M., Sammicheli, S., Rogers, N.C., Sahai, E., Zelenay, S., and Reis E Sousa, C. (2018). NK Cells Stimulate Recruitment of cDC1 into the Tumor Microenvironment Promoting Cancer Immune Control. Cell *172*, 1022–1037.

Cerami, E., Gao, J., Dogrusoz, U., Gross, B.E., Sumer, S.O., Aksoy, B.A., Jacobsen, A., Byrne, C.J., Heuer, M.L., Larsson, E., et al. (2012). The cBio cancer genomics portal: an open platform for exploring multidimensional cancer genomics data. Cancer Discov. *2*, 401–404.

Chen, Y., Zhou, Z., and Min, W. (2018). Mitochondria, Oxidative Stress and Innate Immunity. Front. Physiol. *9*, 1487.

Chow, M.T., and Luster, A.D. (2014). Chemokines in cancer. Cancer Immunol. Res. *2*, 1125–1131.

Cretella, D., Ravelli, A., Fumarola, C., La Monica, S., Digiacomo, G., Cavazzoni, A., Alfieri, R., Biondi, A., Generali, D., Bonelli, M., et al. (2018). The anti-tumor efficacy of CDK4/6 inhibition is enhanced by the combination with PI3K/AKT/mTOR inhibitors through impairment of glucose metabolism in TNBC cells. J. Exp. Clin. Cancer Res. *37*, 72.

Cristescu, R., Mogg, R., Ayers, M., Albright, A., Murphy, E., Yearley, J., Sher, X., Liu, X.Q., Lu, H., Nebozhyn, M., et al. (2018). Pan-tumor genomic biomarkers for PD-1 checkpoint blockade-based immunotherapy. Science *362*, eaar3593.

Cristofanilli, M., Turner, N.C., Bondarenko, I., Ro, J., Im, S.A., Masuda, N., Colleoni, M., DeMichele, A., Loi, S., Verma, S., et al. (2016). Fulvestrant plus palbociclib versus fulvestrant plus placebo for treatment of hormone-receptor-positive, HER2-negative metastatic breast cancer that progressed on previous endocrine therapy (PALOMA-3): final analysis of the multicentre, double-blind, phase 3 randomised controlled trial. Lancet Oncol. *17*, 425–439.

Dangaj, D., Bruand, M., Grimm, A.J., Ronet, C., Barras, D., Duttagupta, P.A., Lanitis, E., Duraiswamy, J., Tanyi, J.L., Benencia, F., et al. (2019). Cooperation between Constitutive and Inducible Chemokines Enables T Cell Engraftment and Immune Attack in Solid Tumors. Cancer Cell *35*, 885–900.

DeNardo, G.L., Mirick, G.R., Hok, S., DeNardo, S.J., Beckett, L.A., Adamson, G.N., and Balhorn, R.L. (2009). Molecular specific and cell selective cytotoxicity induced by a novel synthetic HLA-DR antibody mimic for lymphoma and leukemia. Int. J. Oncol. *34*, 511–516.

Deng, J., Wang, E.S., Jenkins, R.W., Li, S., Dries, R., Yates, K., Chhabra, S., Huang, W., Liu, H., Aref, A.R., et al. (2018). CDK4/6 Inhibition Augments Antitumor Immunity by Enhancing T-cell Activation. Cancer Discov. *8*, 216–233.

Dushyanthen, S., Beavis, P.A., Savas, P., Teo, Z.L., Zhou, C., Mansour, M., Darcy, P.K., and Loi, S. (2015). Relevance of tumor-infiltrating lymphocytes in breast cancer. BMC Med. *13*, 202.

Escola, J.M., Kuenzi, G., Gaertner, H., Foti, M., and Hartley, O. (2010). CC chemokine receptor 5 (CCR5) desensitization: cycling receptors accumulate in the trans-Golgi network. J. Biol. Chem. *285*, 41772–41780.

Finn, R.S., Dering, J., Conklin, D., Kalous, O., Cohen, D.J., Desai, A.J., Ginther, C., Atefi, M., Chen, I., Fowst, C., et al. (2009). PD 0332991, a selective cyclin D kinase 4/6 inhibitor, preferentially inhibits proliferation of luminal estrogen receptor-positive human breast cancer cell lines in vitro. Breast Cancer Res. *11*, R77.

Forrester, S.J., Kikuchi, D.S., Hernandes, M.S., Xu, Q., and Griendling, K.K. (2018). Reactive Oxygen Species in Metabolic and Inflammatory Signaling. Circ. Res. *122*, 877–902.

Franco, J., Balaji, U., Freinkman, E., Witkiewicz, A.K., and Knudsen, E.S. (2016). Metabolic Reprogramming of Pancreatic Cancer Mediated by CDK4/6 Inhibition Elicits Unique Vulnerabilities. Cell Rep. *14*, 979–990.

Goel, S., Wang, Q., Watt, A.C., Tolaney, S.M., Dillon, D.A., Li, W., Ramm, S., Palmer, A.C., Yuzugullu, H., Varadan, V., et al. (2016). Overcoming Therapeutic Resistance in HER2-Positive Breast Cancers with CDK4/6 Inhibitors. Cancer Cell *29*, 255–269.

Goel, S., DeCristo, M.J., Watt, A.C., BrinJones, H., Sceneay, J., Li, B.B., Khan, N., Ubellacker, J.M., Xie, S., Metzger-Filho, O., et al. (2017). CDK4/6 inhibition triggers anti-tumour immunity. Nature *548*, 471–475.

Gogvadze, V., Orrenius, S., and Zhivotovsky, B. (2008). Mitochondria in cancer cells: what is so special about them? Trends Cell Biol. *18*, 165–173.

Griffith, J.W., Sokol, C.L., and Luster, A.D. (2014). Chemokines and chemokine receptors: positioning cells for host defense and immunity. Annu. Rev. Immunol. *32*, 659–702.

Guy, C.T., Cardiff, R.D., and Muller, W.J. (1992). Induction of mammary tumors by expression of polyomavirus middle T oncogene: a transgenic mouse model for metastatic disease. Mol. Cell. Biol. *12*, 954–961.

Harlin, H., Meng, Y., Peterson, A.C., Zha, Y., Tretiakova, M., Slingluff, C., McKee, M., and Gajewski, T.F. (2009). Chemokine expression in melanoma metastases associated with CD8+ T-cell recruitment. Cancer Res. *69*, 3077–3085.

Hurvitz, S.A., Martin, M., Press, M.F., Chan, D., Fernandez-Abad, M., Petru, E., Rostorfer, R., Guarneri, V., Huang, C.S., Barriga, S., et al. (2020). Potent Cell-Cycle Inhibition and Upregulation of Immune Response with Abemaciclib and Anastrozole in neoMONARCH, Phase II Neoadjuvant Study in $HR^{+}/HER2^{-}$ Breast Cancer. Clin. Cancer Res. *26*, 566–580.

Jin, J., and Zhao, Q. (2020). Emerging role of mTOR in tumor immune contexture: Impact on chemokine-related immune cells migration. Theranostics *10*, 6231–6244.

Klein, M.E., Kovatcheva, M., Davis, L.E., Tap, W.D., and Koff, A. (2018). CDK4/6 Inhibitors: The Mechanism of Action May Not Be as Simple as Once Thought. Cancer Cell *34*, 9–20.

Knudsen, E.S., and Witkiewicz, A.K. (2017). The Strange Case of CDK4/6 Inhibitors: Mechanisms, Resistance, and Combination Strategies. Trends Cancer *3*, 39–55.

Kohchi, C., Inagawa, H., Nishizawa, T., and Soma, G. (2009). ROS and innate immunity. Anticancer Res. *29*, 817–821.

Laplante, M., and Sabatini, D.M. (2012). mTOR Signaling. Cold Spring Harb. Perspect. Biol. *4*, a011593.

Li, T., Fu, J., Zeng, Z., Cohen, D., Li, J., Chen, Q., Li, B., and Liu, X.S. (2020). TIMER2.0 for analysis of tumor-infiltrating immune cells. Nucleic Acids Res. *48* (*W1*), W509–W514.

Lin, E.Y., Jones, J.G., Li, P., Zhu, L., Whitney, K.D., Muller, W.J., and Pollard, J.W. (2003). Progression to malignan\cy in the polyoma middle T oncoprotein mouse breast cancer model provides a reliable model for human diseases. Am. J. Pathol. *163*, 2113–2126.

Lin, H.Y., Chang, K.T., Hung, C.C., Kuo, C.H., Hwang, S.J., Chen, H.C., Hung, C.H., and Lin, S.F. (2014). Effects of the mTOR inhibitor rapamycin on monocyte-secreted chemokines. BMC Immunol. *15*, 37.

Liu, G.Y., and Sabatini, D.M. (2020). mTOR at the nexus of nutrition, growth, ageing and disease. Nat. Rev. Mol. Cell Biol. *21*, 183–203.

Lugrin, J., Rosenblatt-Velin, N., Parapanov, R., and Liaudet, L. (2014). The role of oxidative stress during inflammatory processes. Biol. Chem. *395*, 203–230.

Morita, M., Gravel, S.P., Chénard, V., Sikström, K., Zheng, L., Alain, T., Gandin, V., Avizonis, D., Arguello, M., Zakaria, C., et al. (2013). mTORC1 controls mitochondrial activity and biogenesis through 4E-BP-dependent translational regulation. Cell Metab. *18*, 698–711.

Nagarsheth, N., Wicha, M.S., and Zou, W. (2017). Chemokines in the cancer microenvironment and their relevance in cancer immunotherapy. Nat. Rev. Immunol. *17*, 559–572.

Newman, A.M., Liu, C.L., Green, M.R., Gentles, A.J., Feng, W., Xu, Y., Hoang, C.D., Diehn, M., and Alizadeh, A.A. (2015). Robust enumeration of cell subsets from tissue expression profiles. Nat. Methods *12*, 453–457.

O'Brien, N.A., McDermott, M.S.J., Conklin, D., Luo, T., Ayala, R., Salgar, S., Chau, K., DiTomaso, E., Babbar, N., Su, F., et al. (2020). Targeting activated PI3K/mTOR signaling overcomes acquired resistance to CDK4/6-based therapies in preclinical models of hormone receptor-positive breast cancer. Breast Cancer Res. *22*, 89.

Petroni, G., Formenti, S.C., Chen-Kiang, S., and Galluzzi, L. (2020). Immunomodulation by anticancer cell cycle inhibitors. Nat. Rev. Immunol. *20*, 669–679.

Sabatini, D.M. (2017). Twenty-five years of mTOR: Uncovering the link from nutrients to growth. Proc. Natl. Acad. Sci. USA *114*, 11818–11825.

Saxton, R.A., and Sabatini, D.M. (2017). mTOR Signaling in Growth, Metabolism, and Disease. Cell *169*, 361–371.

Schaer, D.A., Beckmann, R.P., Dempsey, J.A., Huber, L., Forest, A., Amaladas, N., Li, Y., Wang, Y.C., Rasmussen, E.R., Chin, D., et al. (2018). The CDK4/6 Inhibitor Abemaciclib Induces a T Cell Inflamed Tumor Microenvironment and Enhances the Efficacy of PD-L1 Checkpoint Blockade. Cell Rep. *22*, 2978–2994.

Scialò, F., Fernández-Ayala, D.J., and Sanz, A. (2017). Role of Mitochondrial Reverse Electron Transport in ROS Signaling: Potential Roles in Health and Disease. Front. Physiol. *8*, 428.

Sozzani, S., Bosisio, D., Mantovani, A., and Ghezzi, P. (2005). Linking stress, oxidation and the chemokine system. Eur. J. Immunol. *35*, 3095–3098.

Spranger, S., Dai, D., Horton, B., and Gajewski, T.F. (2017). Tumor-Residing Batf3 Dendritic Cells Are Required for Effector T Cell Trafficking and Adoptive T Cell Therapy. Cancer Cell *31*, 711–723.

Stoll, G., Pol, J., Soumelis, V., Zitvogel, L., and Kroemer, G. (2018). Impact of chemotactic factors and receptors on the cancer immune infiltrate: a bioinformatics study revealing homogeneity and heterogeneity among patient cohorts. OncoImmunology *7*, e1484980.

Tarrado-Castellarnau, M., de Atauri, P., Tarragó-Celada, J., Perarnau, J., Yuneva, M., Thomson, T.M., and Cascante, M. (2017). *De novo* MYC addiction as an adaptive response of cancer cells to CDK4/6 inhibition. Mol. Syst. Biol. *13*, 940.

Teh, J.L.F., and Aplin, A.E. (2019). Arrested Developments: CDK4/6 Inhibitor Resistance and Alterations in the Tumor Immune Microenvironment. Clin. Cancer Res. *25*, 921–927.

Teh, J.L.F., Cheng, P.F., Purwin, T.J., Nikbakht, N., Patel, P., Chervoneva, I., Ertel, A., Fortina, P.M., Kleiber, I., HooKim, K., et al. (2018). In Vivo E2F Reporting Reveals Efficacious Schedules of MEK1/2-CDK4/6 Targeting and mTOR-S6 Resistance Mechanisms. Cancer Discov. *8*, 1654, 1654.

Tumeh, P.C., Harview, C.L., Yearley, J.H., Shintaku, I.P., Taylor, E.J., Robert, L., Chmielowski, B., Spasic, M., Henry, G., Ciobanu, V., et al. (2014). PD-1 blockade induces responses by inhibiting adaptive immune resistance. Nature *515*, 568–571.

Turner, N.C., Slamon, D.J., Ro, J., Bondarenko, I., Im, S.A., Masuda, N., Colleoni, M., DeMichele, A., Loi, S., Verma, S., et al. (2018). Overall Survival with Palbociclib and Fulvestrant in Advanced Breast Cancer. N. Engl. J. Med. *379*, 1926–1936.

Valcourt, J.R., Lemons, J.M., Haley, E.M., Kojima, M., Demuren, O.O., and Coller, H.A. (2012). Staying alive: metabolic adaptations to quiescence. Cell Cycle *11*, 1680–1696.

Vilgelm, A.E., and Richmond, A. (2019). Chemokines Modulate Immune Surveillance in Tumorigenesis, Metastasis, and Response to Immunotherapy. Front. Immunol. *10*, 333.

Vilgelm, A.E., Johnson, C.A., Prasad, N., Yang, J., Chen, S.C., Ayers, G.D., Pawlikowski, J.S., Raman, D., Sosman, J.A., Kelley, M., et al. (2015a). Connecting the Dots: Therapy-Induced Senescence and a Tumor-Suppressive Immune Microenvironment. J. Natl. Cancer Inst. *108*, djv406.

Vilgelm, A.E., Pawlikowski, J.S., Liu, Y., Hawkins, O.E., Davis, T.A., Smith, J., Weller, K.P., Horton, L.W., McClain, C.M., Ayers, G.D., et al. (2015b). Mdm2 and aurora kinase a inhibitors synergize to block melanoma growth by driving apoptosis and immune clearance of tumor cells. Cancer Res. *75*, 181–193.

Vilgelm, A.E., Johnson, D.B., and Richmond, A. (2016). Combinatorial approach to cancer immunotherapy: strength in numbers. J. Leukoc. Biol. *100*, 275–290.

Vilgelm, A.E., Cobb, P., Malikayil, K., Flaherty, D., Andrew Johnson, C., Raman, D., Saleh, N., Higgins, B., Vara, B.A., Johnston, J.N., et al. (2017). MDM2 Antagonists Counteract Drug-Induced DNA Damage. EBioMedicine *24*, 43–55.

Vilgelm, A.E., Saleh, N., Shattuck-Brandt, R., Riemenschneider, K., Slesur, L., Chen, S.C., Johnson, C.A., Yang, J., Blevins, A., Yan, C., et al. (2019). MDM2 antagonists overcome intrinsic resistance to CDK4/6 inhibition by inducing p21. Sci. Transl. Med. *11*, Published online July 31, 2019. https://doi.org/10.1126/scitranslmed.aav7171.

Warth, B., Raffeiner, P., Granados, A., Huan, T., Fang, M., Forsberg, E.M., Benton, H.P., Goetz, L., Johnson, C.H., and Siuzdak, G. (2018). Metabolomics Reveals that Dietary Xenoestrogens Alter Cellular Metabolism Induced by Palbociclib/Letrozole Combination Cancer Therapy. Cell Chem. Biol. *25*, 291–300.

Warth, B., Palermo, A., Rattray, N.J.W., Lee, N.V., Zhu, Z., Hoang, L.T., Cai, Y., Mazurek, A., Dann, S., VanArsdale, T., et al. (2019). Palbociclib and Fulvestrant Act in Synergy to Modulate Central Carbon Metabolism in Breast Cancer Cells. Metabolites *9*, 7.

Weichhart, T., Hengstschläger, M., and Linke, M. (2015). Regulation of innate immune cell function by mTOR. Nat. Rev. Immunol. *15*, 599–614.

Wellen, K.E., and Thompson, C.B. (2010). Cellular metabolic stress: considering how cells respond to nutrient excess. Mol. Cell *40*, 323–332.

Wellenstein, M.D., and de Visser, K.E. (2018). Cancer-Cell-Intrinsic Mechanisms Shaping the Tumor Immune Landscape. Immunity *48*, 399–416.

William, M., Leroux, L.P., Chaparro, V., Graber, T.E., Alain, T., and Jaramillo, M. (2019). Translational repression of Ccl5 and Cxcl10 by 4E-BP1 and 4E-BP2 restrains the ability of mouse macrophages to induce migration of activated T cells. Eur. J. Immunol. *49*, 1200–1212.

Yarosz, E.L., and Chang, C.H. (2018). The Role of Reactive Oxygen Species in Regulating T Cell-mediated Immunity and Disease. Immune Netw. *18*, e14.

Yoshida, A., Bu, Y., Qie, S., Wrangle, J., Camp, E.R., Hazard, E.S., Hardiman, G., de Leeuw, R., Knudsen, K.E., and Diehl, J.A. (2019). SLC36A1-mTORC1 signaling drives acquired resistance to CDK4/6 inhibitors. Sci. Adv. *5*, eaax6352.

Zanuy, M., Ramos-Montoya, A., Villacañas, O., Canela, N., Miranda, A., Aguilar, E., Agell, N., Bachs, O., Rubio-Martinez, J., Pujol, M.D., et al. (2012). Cyclin-dependent kinases 4 and 6 control tumor progression and direct glucose oxidation in the pentose cycle. Metabolomics *8*, 454–464.

Zhang, J., Bu, X., Wang, H., Zhu, Y., Geng, Y., Nihira, N.T., Tan, Y., Ci, Y., Wu, F., Dai, X., et al. (2018). Cyclin D-CDK4 kinase destabilizes PD-L1 via cullin 3-SPOP to control cancer immune surveillance. Nature *553*, 91–95.

STAR★METHODS

KEY RESOURCES TABLE

REAGENT or RESOURCE	SOURCE	IDENTIFIER
Antibodies		
CD45	BioLegend	103116; RRID:AB_312981
CD3	Fisher	460032-80; RRID:AB_1834428
CD4	BioLegend	100438; RRID:AB_11203718
CD8	BioLegend	100712; RRID:AB_312751
NK1.1	BioLegend	108708; RRID:AB_313395
CD19	Miltenyi	130-105-171; RRID:AB_2661109
CD44	BioLegend	103025; RRID:AB_493712
CD62L	BioLegend	104417; RRID:AB_313102
TIM3	BioLegend	119721; RRID:AB_2616907
LAG3	BioLegend	125219; RRID:AB_2566571
CXCR3	BioLegend	126531; RRID:AB_2563160
CD8a	Thermofisher	46-0081-82; RRID:AB_1834433
CD11C	BioLegend	117330; RRID:AB_11219593
F4/80	Thermofisher	17-4801-80; RRID:AB_2784647
CD206	BioLegend	141705; RRID:AB_10896421
CD11b	BioLegend	101217; RRID:AB_389305
I-A/I-E	BioLegend	107622; RRID:AB_493727
Ly6G	BioLegend	127617; RRID:AB_1877262
Ly-6C	BioLegend	128035; RRID:AB_2562352
CD103	BD	564322; RRID:AB_2738744
PD-L1	BD	740614; RRID:AB_2740313
CD45	BD	564279; RRID:AB_2651134
CD69	Invitrogen	11-0691-85; RRID:AB_465120
FOXP3	BioLegend	126404; RRID:AB_1089117
CD25	Invitrogen	56-0251-80; RRID:AB_891424
MHC Class I	Invitrogen	25-5958-80; RRID:AB_2573504
CD137	Invitrogen	46-1371-80; RRID:AB_2573713
CD134	BD	740945; RRID:AB_2740573
CD3e	BD	563024; RRID:AB_2737959
CD8	BioLegend	100712; RRID:AB_312751
CD11b	BioLegend	101267; RRID:AB_2810328
CD8-depleting antibody (YTS 169.4)	BioXcell (West Lebanon, NH)	BP0117; RRID:AB_10950145
Anti-OX-40 (OX-86)	BioXcell (West Lebanon, NH)	BE0031; RRID:AB_1107592
Anti-4-1BB (LOB12.3)	BioXcell (West Lebanon, NH)	BP0169; RRID:AB_10949016
Purified anti-mouse CD183 (CXCR3)	Biolegend	126502; RRID:AB_1027635
Anti-CD3e	Biolegend	100302; RRID:AB_312667
Anti-CD28	Biolegend	102102; RRID:AB_312867
Anti-mouse CD16/32	Biolegend	156604; RRID:AB_2783138
RB1	Cell signaling	9309S; RRID:AB_823629
Phospho- RB (S807/S811) rabbit antibody	Cell signaling	8516S; RRID:AB_11178658
S6 Ribosomal protein rabbit antibody	Cell signaling	2217S; RRID:AB_331355
Phospho-S6 (S235/236) Ribosomal protein rabbit antibody	Cell signaling	2211S; RRID:AB_331679

(*Continued on next page*)

Continued

REAGENT or RESOURCE	SOURCE	IDENTIFIER
Phospho-S6 (S240/244) ribosomal protein rabbit antibody	Cell signaling	5364; RRID:AB_10694233
Phospho-p70 S6 (T389) kinase rabbit antibody	Cell signaling	9234; RRID:AB_2269803
p70 S6 kinase rabbit antibody	Cell signaling	2708; RRID:AB_390722
p21 Waf1/Cip1 rabbit antibody	Cell signaling	2947S; RRID:AB_823586
β-actin rabbit antibody	Cell signaling	4970S; RRID:AB_2223172
β-tubulin rabbit antibody	Cell signaling	2146S; RRID:AB_2210545
HSP90 rabbit antibody	Cell signaling	4874S; RRID:AB_2121214
Chemicals, peptides, and recombinant proteins		
Dulbecco's modified Eagle's medium/F12	GIBCO	11330032
GlutaMAX	GIBCO	35050061
GIBCO Penicillin-Streptomycin	GIBCO	15-140-122
Fetal Bovine Serum	GIBCO	16000036
Palbociclib	Pfizer	N/A
Palbociclib	LC laboratories	P-7766
Rapamycin	Tocris	1292
N-acetylcysteine	Sigma	A9165
benzylserine	Sigma	13900
Bay876	Sigma	SML1774
BKM120	Sigma	10296
Maraviroc	Adooq	A10556
CellTracker Green CMFDA Dye	Invitrogen	C2925
Murine recombinant CCL5	Peprotech	25007
MitoTracker Green	Invitrogen	T7514
CellRox Deep Red	Invitrogen	C10422
LysoTracker Deep Red	Invitrogen	L12492
DAPI	Invitrogen	D1306
Hoechst 33342	Invitrogen	H1399
JC-1 Mitochondrial Membrane Potential Dye	Thermo Fisher	3168
Fixable Viability Dye eFluor 780	Invitrogen	65-0865-14
LIVE/DEAD Fixable Aqua Dead Cell Stain Kit	Thermofisher	L34957
Everolimus	LC Laboratories	E-4040
10X Tris/Glycine/SDS Buffer	Biorad	1610772
Tris Buffer Saline	Fisher Bioreagents	BP2471-1
Tween 20	Fisher Bioreagents	BP 337-500
Trans Blot Turbo RTA transfer kit	Biorad	170-4270
Bovine serum Albumin	Fisher Bioreagents	BP9706-100
Protein assay dye reagent concentrate	Biorad	5000006
Critical commercial assays		
Reverse Phase Protein Array (RPPA)	Core Facility at MD Anderson Cancer Center (Houston, TX)	N/A
RNA-easy mini kit	QIAGEN	74104
iScript cDNA synthesis kit	BioRad	1708890
Quantiline ELISA HumanCXCL10/IP-10	R&D system	DIP100
Quantiline ELISA Human CCL5/RANTES	R%D system	DRN00B

(*Continued on next page*)

Continued

REAGENT or RESOURCE	SOURCE	IDENTIFIER
Tumor tissue dissociation kit	Miltenyi Biotech	130-096-730
FXP3/ Transcription Factor Staining Buffer Set	Invitrogen	00-5523-00
SYBR-green master mix	BioRad	1725270
Senescence β-Galactosidase Staining Kit	Sigma	CS0030
Experimental models: Cell lines		
MCF7 Cell line	American Type Culture Collection	ATCC HTB22
Cal120 cell line	Carlos L. Arteaga Vanderbilt-Ingram Cancer Center.	N/A
MDA-MB-453 cell line	Carlos L. Arteaga Vanderbilt-Ingram Cancer Center.	N/A
MDA-MB-468 cell line	Carlos L. Arteaga Vanderbilt-Ingram Cancer Center.	N/A
HCC70 cell line	Carlos L. Arteaga Vanderbilt-Ingram Cancer Center.	N/A
BT20 cell line	Carlos L. Arteaga Vanderbilt-Ingram Cancer Center.	N/A
PYMT cell line	Philip Owens (VA Eastern Colorado Health Care System, Denver, CO)	N/A
PYMT-OVA cell line	David DeNardo (Washington University St. Louis, St. Louis MO)	N/A
Experimental models: Organisms/strains		
C57BL/6 mice	The Jackson Laboratory	000664
C57BL/6 mice	Charles River/NCI	Strain code:027
OT-1 mice	Marc Boothby, Richard O'Neil (Vanderbilt University, Nashville, TN)	N/A
OT-1 mice	The Jackson Laboratory	003831
FVB-PYMT transgenic mice	Harold Moses (Vanderbilt University, Nashville, TN)	N/A
Oligonucleotides		
Primer: h CXCL10 F GTGGCATTCAAGGAGTACCTC	Sigma	N/A
Primer: h CXCL10 R TGATGGCCTTCGATTCTGGATT	Sigma	N/A
Primer: h CXCL9 F CCAGTAGTGAGAAAGGGTCGC	Sigma	N/A
Primer: h CXCL9 R AGGGCTTGGGGCAAATTGTT	Sigma	N/A
Primer: m CXCL9 F GGAGTTCGAGGAACCCTA	Sigma	N/A
Primer: m CXCL9 R GGGATTTGTAGTAGTGGATCGTGC	Sigma	N/A
Primer: m CCL5 F GCTGCTTTGCCTACCTCTCC	Sigma	N/A
Primer: m CCL5 R TCGAGTGACAAACACGACTGC	Sigma	N/A
Primer: h CCL5 F CCAGCAGTCGTCTTTGTCAC	Sigma	N/A
Primer: h CCL5 R CTCTGGGTTGGCACACACTT	Sigma	N/A

(*Continued on next page*)

Continued

REAGENT or RESOURCE	SOURCE	IDENTIFIER
Software and algorithms		
ImageJ	NIH Image	https://imagej.nih.gov/ij/index.html
Graphpad's Prism 7.03 software	GraphPad	https://www.graphpad.com/
R (version3.3.0.)	Bioconductor	https://www.bioconductor.org/packages/devel/bioc/vignettes/limma/inst/doc/usersguide.pdf
Timer version 2.0	Li et al., 2020	http://timer.cistrome.org/
Morpheus	Broad Institute	https://software.broadinstitute.org/morpheus/
cBioPortal for Cancer Genomics version 3.6.3	Cerami et al., 2012	https://www.cbioportal.org/

RESOURCE AVAILABILITY

Lead contact

Further information and requests for all original resources and reagents presented in this manuscript should be directed to and will be fulfilled by the Lead contact, Anna Vilgelm (anna.vilgelm@osumc.edu).

Materials availability

This study did not generate new unique reagents.

Data and code availability

The published article includes all datasets generated during this study. Original data for Figure 4A is available in supplemental spreadsheet 1.

EXPERIMENTAL MODEL AND SUBJECT DETAILS

Mice

All animal experiments were approved by Vanderbilt University and the Ohio State University IACUC. Female mice were used in this study as breast cancer primarily affects female population. For transplanted model, mice were 7-14 weeks of age at the time of tumor inoculation. Transgenic PYMT mice were 8-13 weeks of age at the time of treatment initiation. To inoculate tumors in female C57BL/6 mice, 100,000 PYMT or PYMT-Ova tumor cells were injected into 4^{th} mammary fat pad as specified in figure legends. Palbociclib was administered by oral gavage at 100 mg/kg once or twice per day as indicated in figure legends. Palbociclib oral solution was prepared in 0.5% methylcellulose. OX-40 and 4-1BB agonistic antibodies and CD8-depleting antibody were diluted in PBS and administered by intraperitoneal injection at 100 μg/mouse. Injections were given every 3 days for a total of 4 doses. OT-1 cells were suspended in PBS and administered via retro-orbital injection at $8x10^6$ cells per mouse. For *in vivo* chemokine receptor blockade studies mice were treated with 10 mg/kg CCR5i maraviroc (once a day by oral gavage) or CXCR3-blocking antibody (200 μg/mouse, intraperitoneal injection every 3 days). mTORi everolimus was administered via oral gavage once a day at 5mg/kg. Mouse body weight was assessed once a week, and tumor dimensions were measured twice a week with microcalipers (Fisherbrand Traceable). Tumor volume was calculated as 0.5 × length × width × width. Treatment began when tumors reached 50 to 150 mm^3 volume on average. Mice were sacrificed when tumors exceeded 15 mm in diameter or became perforated.

Cell lines

MCF7 cells were purchased from the American Type Culture Collection. Cal120, MDA-MB-453, MDA-MB-468, HCC70, and BT20 cells were provided by Carlos Arteaga. PYMT murine mammary tumor cells syngeneic to C57BL/6 mice were provided by Philip Owens (VA Eastern Colorado Health Care System, Denver, CO). PYMT-OVA cells syngeneic to C57BL/6 mice were provided by David DeNardo (Washington University St. Louis, St. Louis MO). Cells were cultured in Dulbecco's modified Eagle's medium/F12 medium supplemented with 4.5g/L D-Glucose, L-Glutamine, 10% fetal bovine serum (FBS) and 1% penicillin-streptomycin or 100x diluted Anti-Anti mixture (all from GIBCO).

METHOD DETAILS

T cell activation and labeling

To activate T cells for ACT experiments, cells from spleens and lymph nodes of OT-1 mice were plated in 6-well plates coated with anti-CD3e Abs (5μg/mL, overnight at +4, clone 145-2C11, Biolegend) at $2x10^6$ cells per well and incubated further in the presence of

soluble anti-CD28 Abs (3 μg/mL, 37.51, Biolegend) for two days. Next, cells were collected and re-plated at $0.25x10^6$ cells per well and incubated with 12.5 ng/ml of human recombinant IL-2 for another 3 days. Thirty minutes before injection into mice cells were labeled with CellTracker Green CMFDA Dye (ThermoFisher Scientific) as recommended by the manufacturer. To block chemokine-mediated trafficking, OT-1 cells were pre-treated with 100 ug/ml CXCR3-blocking antibody (clone CXCR3-173, Biolegend) or 500nM of murine recombinant CCL5 (Peprotech) for 1 hour before injection. Two hours post injections, mice were sacrificed, and tumors were analyzed for the presence of fluorescent cells using microscopy and flow cytometry.

Chemokine expression analysis

For mRNA expression analysis, RNA was extracted using RNA-easy mini kit (Quiagen). cDNA was prepared from 1 μg of RNA using iScript cDNA synthesis kit (Bio-rad). We used 2 μL of cDNA as a template for Real- Time PCR with SYBR-green master mix (Molecular Probes) and primers specific to CCL5, CXCL9, CXCL10, and β-actin purchased from Sigma. Primer sequences were obtained from PrimerBank[70] (https://pga.mgh.harvard.edu/primerbank/). For analysis of secreted chemokines, ELISA kits for human CXCL10 (IP10) and CCL5 (RANTES), and mouse CXCL9 and CCL5 from Peprotech (Rocky Hills, NJ) or R&D (Minneapolis, MN) were utilized as instructed by the manufacturer. Human chemokine array was purchased from RayBiotech (Peachtree Corners, GA).

Proteomics and western blot

Cells were pelleted by centrifugation at 15000 g and sent to Reverse Phase Protein Array (RPPA) Core Facility at MD Anderson Cancer Center (Houston, TX) for lysis and RPPA analysis. RPPA protein expression was compared between CDK4/6i-treated and vehicle-treated cells using multiple t test without adjusting for multiple comparisons. Threshold for proteins that were reported as up- or downregulated was set at the level of $\geq$ 1.5-fold change and $p < 0.05$. MORPHEUS web tool (https://software.broadinstitute.org/morpheus) was used for clustering of hits and heatmap plotting.

Western blot was performed as described previously (Vilgelm et al., 2017). Antibodies were purchased from Cell Signaling and used as recommended by the vendor. Primary antibodies were applied overnight at 1:500 dilution and secondary antibody were hybridized for 2 hours at 1:5000 dilutions.

Flow cytometry

For detection of immune cells, tumors were excised, dissected into small pieces, and enzymatically digested using tumor tissue dissociation kit (Miltenyi, Germany) according to manufacturer's recommendations. Cells were processed for viability staining using LIVE/DEAD Fixable Aqua Dead Cell Stain Kit or eBioscience Fixable Viability Dye eFluor 780 (Thermofisher) according to manufacturer's instruction. Next, Fc receptor blocking was performed using Purified Rat Anti-Mouse CD16/CD32 Abs (BD biosciences) for 30 min followed by staining with fluorescently labeled antibodies to immune cell surface markers. Information on panels of antibodies, clones, fluorophores, and vendors is provided in Key resources table. For experiments where Fox3 was evaluated, cells were processed using eBioscience Foxp3 / Transcription Factor Staining Buffer Set (Thermofisher). After staining, cells were fixed in 0.5% buffered formaldehyde and analyzed on 4-laser Fortessa (BD Biosciences) for immunophenotyping panels, and on 5-laser Cytek Aurora (Cytek Biosciences) for T cell phenotype panel. Gating and t-SNE dimension reduction was done using FlowJo. In a separate series of *in vitro* experiments, flow cytometry was utilized to determine relative cell size using forward scatter (FSC) and cell complexity using side scatter (FSC). Amount of mitochondria were analyzed using MitoTracker Green (Invitrogen), respectively. Intracellular ROS levels were detected using CellRox Deep Red (Invitrogen) according to manufacturer's recommendation.

Fluorescence and bright-field microscopy

IHC staining was performed by Translational Pathology Shared Resources at Vanderbilt University (Nashville, TN). MitoTracker Green, LysoTracker Deep Red, DAPI, and CellRox Deep Red (all from Invitrogen) were used for fluorescent labeling of mitochondria, lysosomes, nuclei, and intracellular ROS, respectively. Senescence Cells Histochemical Staining Kit (Sigma-Aldrich) was used to detect SA-βGal-positive cells. To detect dead cells and cell DNA in live or dead cells Propidium Iodide (1μg/mL) and Hoechst 33342 (2μg/mL) were added directly into the cell media 20 minutes prior to imaging. JC-1 Mitochondrial Membrane Potential Dye was purchased from Thermofisher and used in accordance with manufacturer's recommendations. To visualize stained tumor sections, cell populations, and intracellular content, EVOS M5000 digital inverted microscope (Thermo Fisher Scientific, Carlsbad, CA, USA) was utilized.

TCGA analysis

To study the association of CCL5 and CXCL10 expression with CD8+ T cell infiltration, Timer2.0 web resource for systematical analysis of immune infiltrates was used (http://timer.cistrome.org/). Expression of chemokines was correlated to CD8+ T cell infiltration estimated by CIBERSORT-Abs., which is a score of arbitrary units that reflects the absolute proportion of each cell type derived from computational analysis of the expression signatures of cell population of interest (Newman et al., 2015). TCGA breast cancer dataset (BRCA) was analyzed.

To query the association of CCL5 and CXCL10 chemokine expression with breast cancer patient survival or phosphorylation of mTOR target protein S6, cBioPortal was used (Cerami et al., 2012). TCGA Breast Invasive Carcinoma Firehose Legacy dataset

was used for analysis. Samples with CCL5 and/or CXCL10 mRNA expression z-scores > 1 were categorized as high expressing, and samples with z-cores < 1 as low-intermediate expressing.

QUANTIFICATION AND STATISTICAL ANALYSIS

Standard t test and one-way ANOVA were used for analysis comparing two samples and multiple samples, respectively. To study the effect of two parameters (i.e., time and treatment) and their interaction, two-way ANOVA was applied. GraphPad's Prism 7.03 software and R (version 3.3.0.) were used for statistical analysis. For *in vivo* experiments, we compared the progression of tumor volume (mm^3) over time among groups of mice receiving different therapy with a linear mixed-effects regression model. To meet the normality assumptions for these parametric methods, a square root or a natural log transformation was implemented to ameliorate the heterogeneity evident in the data. Mixed models estimate corrected variance estimates in the presence of correlated measurements taken in the same mouse (such as left and right flank) and for repeated-measures on the same tumor over time. The Akaike information criterion was used to select among competing correlation structures. Standard residual analysis and goodness-of-fit statistics were evaluated. Survival curves were plotted and compared using GraphPad's Prism. All tests of statistical significance were two sided. The numbers of mice and biological relocates in experimental groups are indicated in figure legends. Animal experiments were performed once, except for experiments combining CDK4/6i with adoptive T cell transfer (Figure 2G) and anti-OX-40/4-1BB (Figure 2A) that were repeated twice with consistent results. *In vitro* experiments were repeated at least 3 times. Error bars represent standard deviation, except for graphs showing tumor volume change over time, where error bars represent standard error.

Cell Reports, Volume *35*

Supplemental information

Metabolic modulation by CDK4/6 inhibitor promotes chemokine-mediated recruitment of T cells into mammary tumors

Roman V. Uzhachenko, Vijaya Bharti, Zhufeng Ouyang, Ashlyn Blevins, Stacey Mont, Nabil Saleh, Hunter A. Lawrence, Chengli Shen, Sheau-Chiann Chen, Gregory D. Ayers, David G. DeNardo, Carlos Arteaga, Ann Richmond, and Anna E. Vilgelm

Table S1. Related to Figure 1. Comparison of the immune cell infiltrate in PYMT tumors from mice treated with vehicle or with CDK4/6i palbociclib (Palbo). ns – not significant, n/t – not tested, TAM – tumor associated macrophage, MDSC – myeloid-derived suppressor cell

Cell population	**Markers (gated on live CD45+ cells)**	**Day 8: Average frequency ± SD (% of CD45+)**		**Day 25: Average frequency ± SD (% of CD45+)**		**Palbo effect**	**Palbo effect p value**	**Day effect p value**	**Interaction p value**
		Vehicle n=9	**Palbo n=9**	**Vehicle n=6**	**Palbo n=6**				
B cells	$CD19^+$	1.78 ± 0.77	3.72 ± 1.49	3.70 ± 1.95	7.17 ± 2.69	increase	0.0003	0.0003	ns
NKT	$NK1.1^+/CD3^+$	5.05 ± 1.05	6.06 ± 1.56	3.22 ± 1.39	2.71 ± 1.22	ns	0.615	<0.0001	ns
NK	$NK1.1^+/CD3^-$	5.34 ± 2.99	5.58 ± 1.57	3.01 ±	2.41 ±	ns	0.802	0.0008	ns
T	$CD3^+$	22.42 ± 4.52	29.35 ± 4.58	28.39 ± 9.68	41.46 ± 13.08	increase	0.002	0.005	ns
CD4	$CD4^+/CD3^+$	7.55 ± 1.32	8.58 ± 2.00	11.48 ± 3.08	14.31 ± 8.41	ns	0.221	0.004	ns
LAG3 CD4	$LAG3^+/CD4^+/CD3^+$	0.72 ± 0.24	0.88 ± 0.42	1.87 ± 0.87	3.72 ± 1.31	increase	0.001	<0.0001	0.005
TIM3 CD4	$TIM3^+/CD4^+/CD3^+$	1.08 ± 0.44	0.71 ± 0.2	2.89 ± 1.29	1.47 ± 0.90	decrease	0.003	<0.0001	ns
CD8	$CD8^+/CD3^+$	5.95 ± 1.53	9.17 ± 2.14	4.05 ± 1.53	7.78 ± 6.65	increase	0.01	ns	ns
LAG3 CD8	$LAG3^+/CD8^+/CD3^+$	0.78 ± 0.52	0.59 ± 0.29	1.04 ± 0.88	1.37 ± 0.57	ns	0.743	0.02	ns
TIM3 CD8	$TIM3^+/CD8^+/CD3^+$	0.86 ± 0.63	0.84 ± 0.44	0.36 ± 0.42	0.51 ± 0.32	ns	0.63	0.029	ns
CD11b	$CD11b^+$	61.22 ± 9.93	55.47 ± 3.83	60.48 ± 9.35	50.48 ± 16.56	decrease	0.049	ns	ns
Macrophages/ TAM	$F4/80^+$	13.78 ± 3.70	12.53 ± 1.46	14.45 ± 3.63	7.57 ± 2.93	decrease	0.001	ns	0.019
CD206 Macroph. (M2 like)	$CD206+/F4/80^+$	5.25 ± 2.71	5.38 ± 1.24	4.16 ± 1.27	2.64 ± 1.11	ns	0.317	0.009	0.231
MHCII Macroph. (M1 like)	$I\text{-}A/I\text{-}E+/F4/80^+$	4.15 ± 1.91	3.27 ± 0.92	5.46 ± 1.74	1.95 ± 1.16	decrease	0.0005	ns	0.026
Monocytes/ mMDSC	$Ly6C^{high}/CD11b^+$	25.83 ± 5.02	20.66 ± 2.49	22.8 ± 2.27	16.87 ± 6.15	decrease	0.002	0.04	ns
Neutrophils/ gMDSC	$Ly6G^{high}/CD11b^+$	1.99 ± 1.08	3.46 ± 1.36	5.89 ± 3.10	14.7 ± 4.95	increase	<0.0001	<0.0001	0.001
PD-L1+ leukocytes	$PD\text{-}L1^+$	33.86 ± 6.81	39.94 ± 8.63	n/t	n/t	ns	0.104	n/t	n/t

Supplementary figures

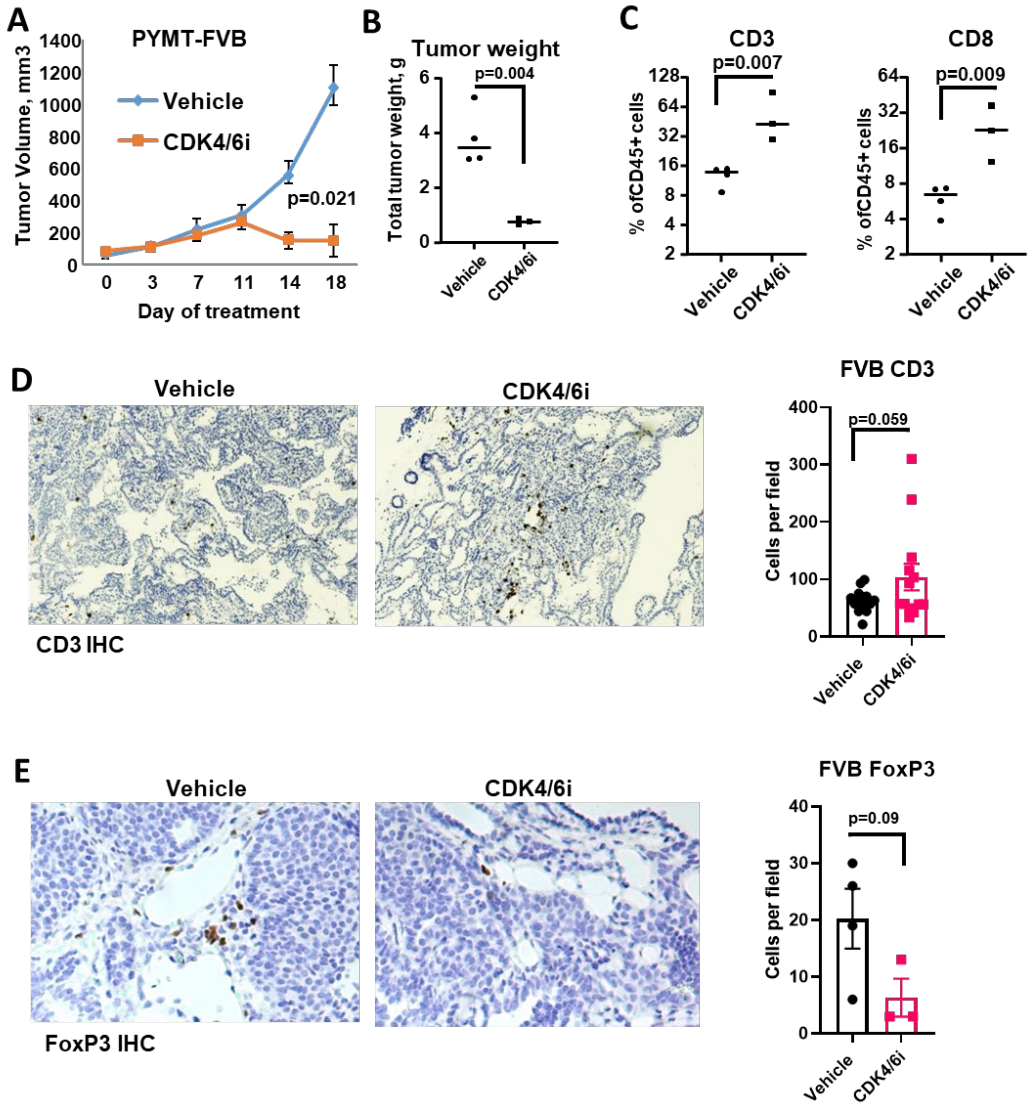

Supplementary Figure 1. Related to Figure 1. Palbociclib inhibits tumor growth and increases T cell infiltrate in transgenic PYMT model of breast cancer. A. Growth of spontaneous mammary tumors in PYMT FBV transgenic mice that were treated twice daily with vehicle or 100mg/kg palbociclib. Growth curves were built based on average volume of all fat pad tumor lesions per mouse (n=3-4 per group, mixed model, data are presented as mean total tumor volume ± SEM). **B.** Comparison of the total weight of all tumor lesions per mouse in vehicle and palbociclib-treated mice using t-test (n=3-4). **C.** Percentages of CD3+ and CD3+/CD8+ cells in tumors of mice shown in A (n=3-4 mice, t-test). **D.** Representative microphotographs and quantification of CD3 IHC staining in tumors of transgenic PYMT FVB mice shown in A. Several random microscopic fields were acquired. Each dot represents a field (n=13-16 fields, t-test). **E.** Representative microphotographs and quantification of FoxP3 IHC staining in tumors of transgenic PYMT FVB mice shown in A (n=3-4 tumors, t-test).

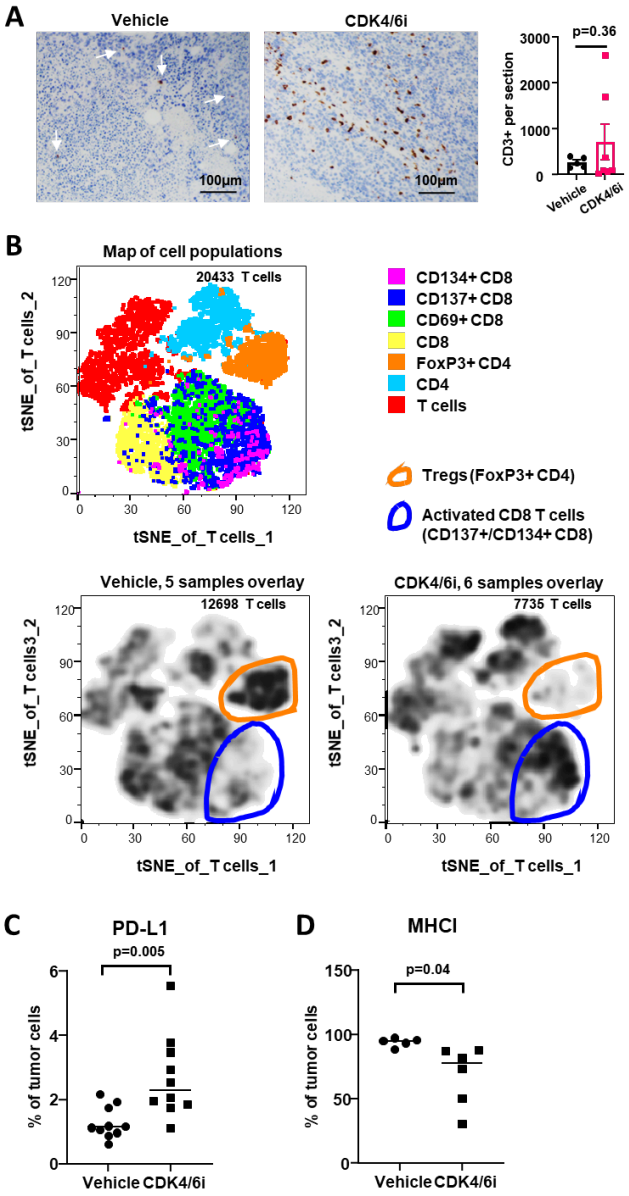

Supplementary Figure 2. Related to Figure 1. Palbociclib affects the levels and phenotype of tumor-infiltrating T cells and surface expression of receptors involved in tumor-immune interaction on malignant cells *in vivo*. A. Representative microphotographs and quantification of CD3 IHC staining in PYMT tumors from female C57Bl/6 mice treated with vehicle or 100 mg/kg palbociclib. Arrows point out infrequent CD3+ cells in vehicle treated group (n=5-7 individual tumors, t-test). **B.** Results of the dimension reduction analysis to visualize overall state of T cell phenotypes in tumors of vehicle and palbociclib-treated mice. These results complement individual parameter data shown in Fig. 1F-K. Populations of Tregs and activated CD8+ T cells are circled. **C.** Results of the flow cytometry analysis of PD-L1 expression of tumor cells from mice shown in Fig. 1F. Tumors were collected at 8-day time points (n=9, t-test). **D.** Results of the flow cytometry analysis of MHC class I expression on tumor cells from experiment described in Fig. 1F (n=5-6 individual tumors, t-test).

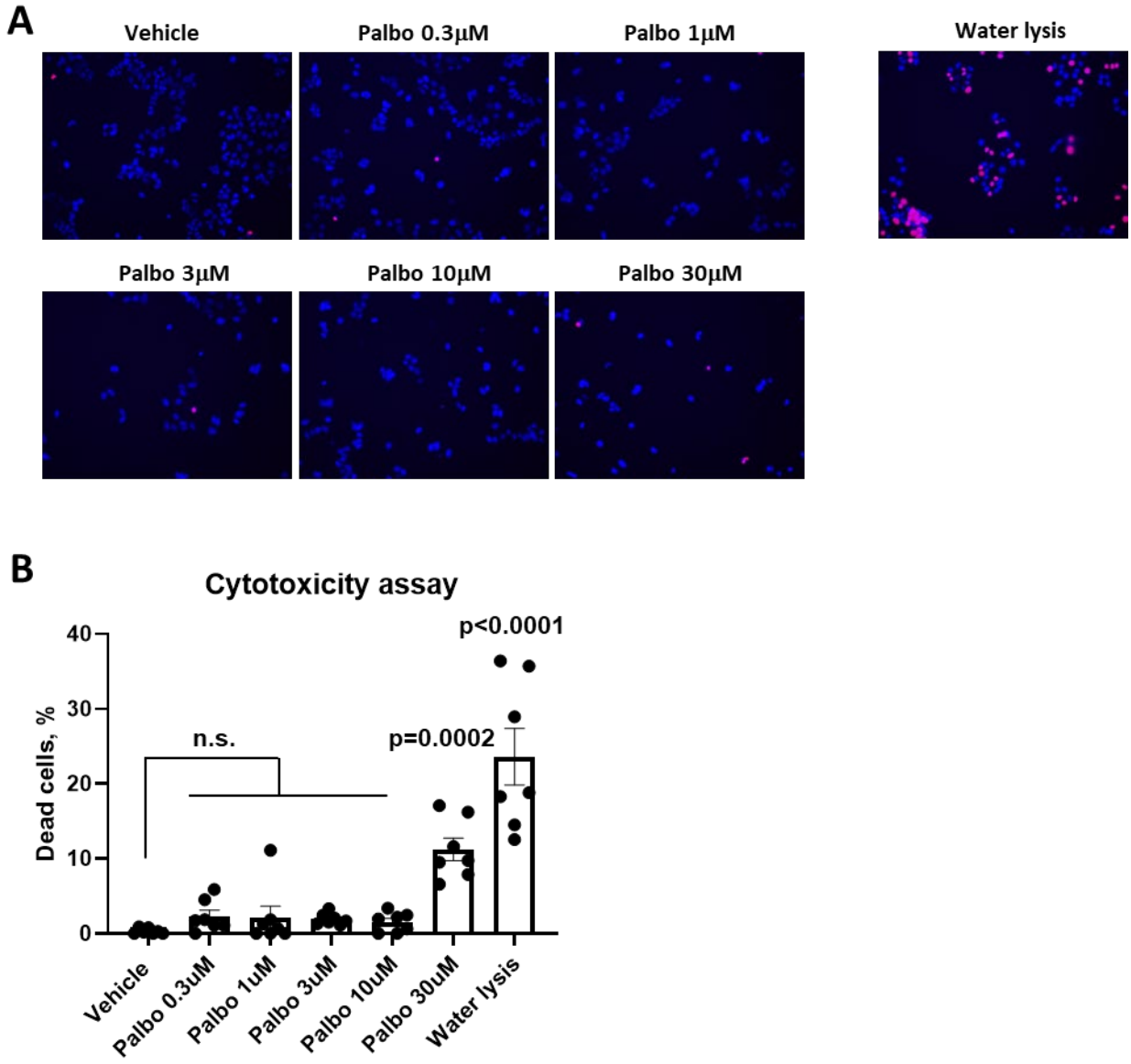

Supplementary Figure 3. Related to Figure 3. Palbociclib is not cytotoxic at 0.3-10µM concentrations. MCF7 cells were treated for 5 days with vehicle or CDK4/6i palbociclib at indicated concentrations. Control cells were killed by incubation in water for 10 min. Dead cells were visualized with PI and all cells were identified by hoechst 33342 staining. A. Representative microphotographs of treated cells. B. Percentages of dead cells in indicated treatment groups counted in random fields (n=7 random fields, one-way ANOVA).

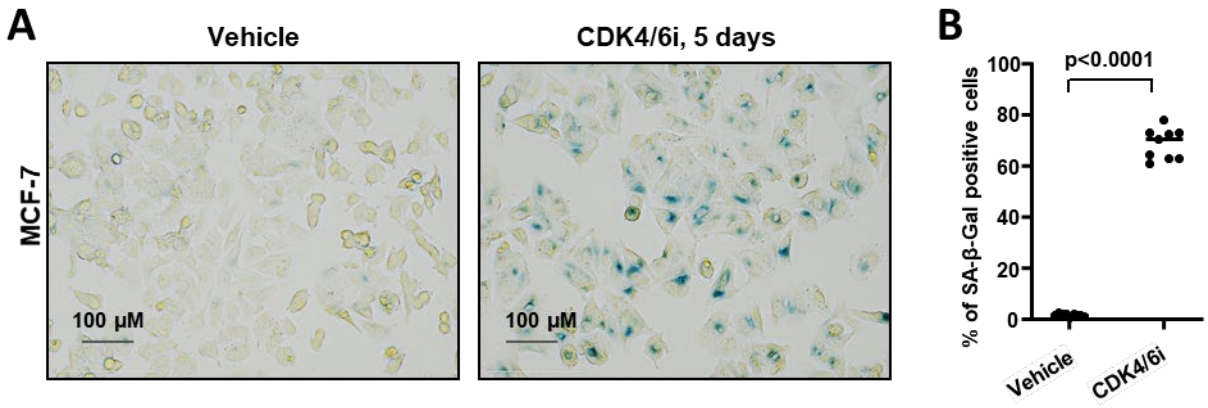

Supplementary Figure 4. Related to Figure 3. Palbociclib induces senescence marker expression in breast cancer cells. A. Images of MCF7 cells cultured in the presence of 1 µM palbociclib for either 8 days or for 5 days followed by drug washout and additional 3 days of culture with drug vehicle only. Control cells were treated with vehicle for 8 days. **B.** Representative images of MCF7 cells treated with vehicle or 1 µM of CDK4/6i palbociclib for 5 days and analyzed for the presence of senescence-associated β-galactosidase. **C.** Statistical analysis of the percentages of senescence-associated β-galactosidase-positive cells (n=9, t- test).

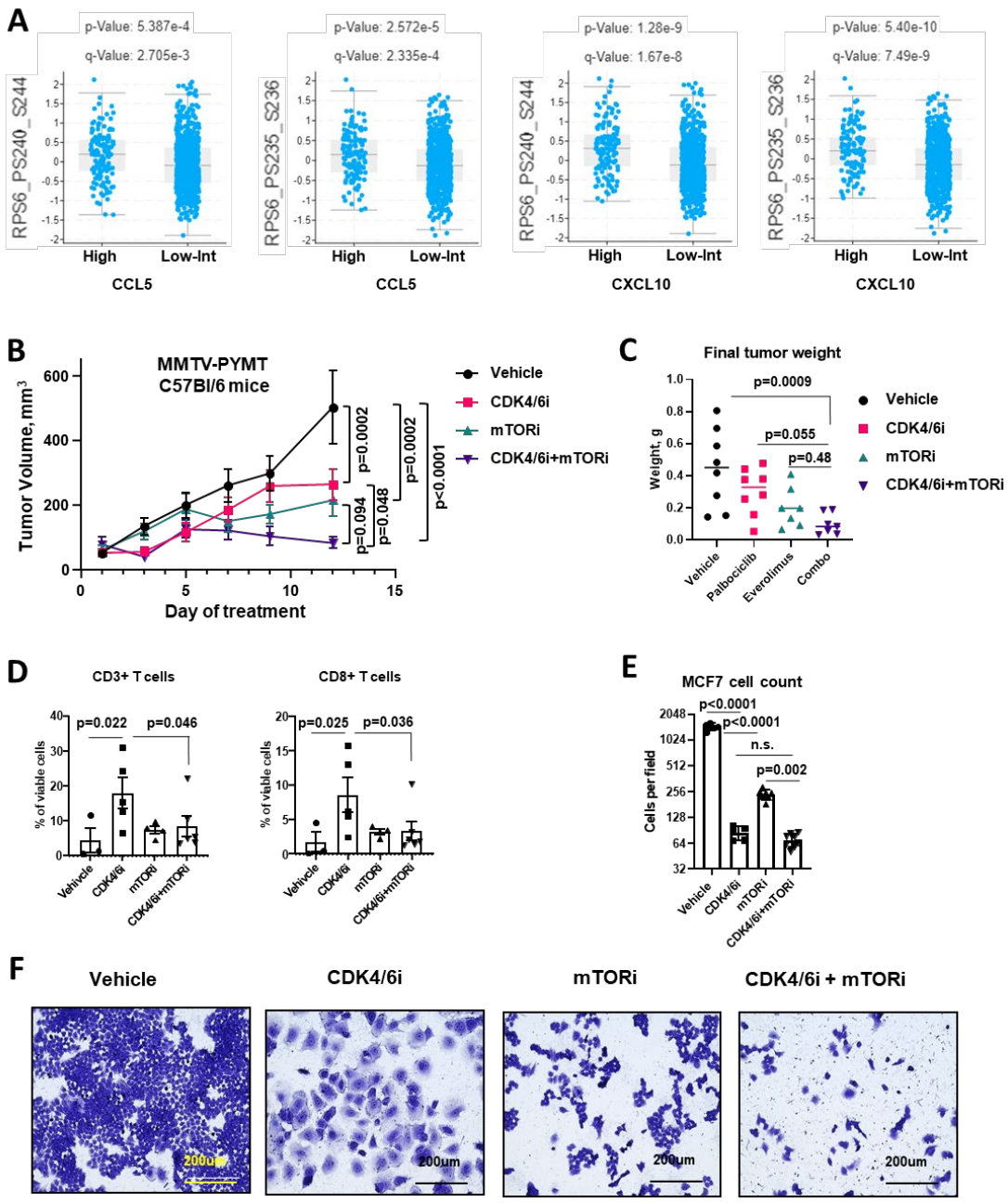

Supplementary Figure 5. Related to Figure 4. Effect of combined mTOR and CDK4/6 blockade on tumor growth and T cell recruitment. A. cBIO portal analysis of the phosphorylation of mTOR target pS6 on residues S240/244 and S235/236 in human breast cancer tumors expressing high vs low-intermediate levels of CCL5 and CXCL10 (n=960, TCGA dataset). **B.** Growth of injected PYMT tumors in female c57Bl/6 mice treated once a day with 100 mg/kg CDK4/6i palbociclib, 5 mg/kg mTORi everolimus, combination of both or vehicle for 12 days (n=6-7, mixed model, error bars represent SEM). **C.** Final tumor weight from experiment described in B. **D.** Results of the flow cytometry analysis of CD3+ (pan-T), and CD3+CD8+ (cytotoxic T cells) cells in tumor cell suspensions from PYMT tumor-bearing C57Bl/6 mice treated with 100 mg/kg CDK4/6i palbociclib, 5 mg/kg mTORi everolimus, combination of both, or vehicle for 8 days. Cells were gated on live cells based on viability dye staining (n=3-6, one-way ANOVA). **E.** Numbers of MCF7 cells treated with 2μM mTOR inhibitor rapamycin (mTORi), 5μM CDK4/6i palbociclib, or combination of both for 5 days. Cells were counted in random microscopic fields after crystal violet staining (n=6, t-test). **F.** Representative microphotographs of cells from experiment in E.